DEVELOPMENTAL BIOLOGY

Aberrant cell state plasticity mediated by developmental reprogramming precedes colorectal cancer initiation

Pratyusha Bala[1,2,3]†, Jonathan P. Rennhack[1,2,3]†, Daulet Aitymbayev[1,3]‡, Clare Morris[1]‡, Sydney M. Moyer[1,2,3], Gina N. Duronio[1], Paul Doan[1], Zhixin Li[1,2,3], Xiaoyan Liang[4], Jason L. Hornick[5], Matthew B. Yurgelun[1,2,6], William C. Hahn[1,2,3], Nilay S. Sethi[1,2,3,6]*

Cell state plasticity is carefully regulated in adult epithelia to prevent cancer. The aberrant expansion of the normally restricted capability for cell state plasticity in neoplasia is poorly defined. Using genetically engineered and carcinogen-induced mouse models of intestinal neoplasia, we observed that impaired differentiation is a conserved event preceding cancer development. Single-cell RNA sequencing (scRNA-seq) of premalignant lesions from mouse models and a patient with hereditary polyposis revealed that cancer initiates by adopting an aberrant transcriptional state characterized by regenerative activity, marked by *Ly6a* (Sca-1), and reactivation of fetal intestinal genes, including *Tacstd2* (Trop2). Genetic inactivation of Sox9 prevented adenoma formation, obstructed the emergence of regenerative and fetal programs, and restored multilineage differentiation by scRNA-seq. Expanded chromatin accessibility at regeneration and fetal genes upon Apc inactivation was reduced by concomitant Sox9 suppression. These studies indicate that aberrant cell state plasticity mediated by unabated regenerative activity and developmental reprogramming precedes cancer development.

INTRODUCTION

Cell state plasticity, the ability of cells to acquire new states via differentiation programs, is a critical cellular feature of embryogenesis, allowing for tissue specification during development (*1*), and adult homeostasis, enabling tissue repair and regeneration (*2*). While cellular plasticity progressively decreases during development, it remains a normal albeit restricted feature of adult epithelial cells that facilitates adaptation to injury and inflammation, among other forms of stress. Eukaryotes rely on epigenetic governance among other layers of regulation to endow cell state plasticity while avoiding properties that permit neoplasia (*3*). Recent studies are providing key evidence that unrestricted cellular plasticity underlies neoplastic initiation, molecular heterogeneity, and suboptimal response to therapy (*4–8*). Impaired differentiation is a key mechanism by which neoplastic cells unlock cell state plasticity (*6, 9*). While differentiation blocks are a well-studied aspect of premalignant hematological conditions and leukemogenesis, their importance in colorectal cancer (CRC) is lesser appreciated.

The rapidly renewing adult intestinal epithelium engenders inherent cellular plasticity. Crypt-restricted Lgr5+ intestinal stem cells (ISCs) and their immediate progeny replicate frequently to spawn a steady stream of postmitotic differentiated cells that function in barrier protection, nutrient absorption, and hormone secretion in the villus before dying (*10*). The key pathways regulating renewal and differentiation include wingless/integrated (WNT) and bone morphogenetic protein (BMP) signaling cascades, respectively. WNT pathway activity maintains stem cell reservoirs and crypt homeostasis, whereas BMP signaling supports the differentiation of progenitors into mature enterocytes, establishing a crypt-villus gradient (Fig. 1A) (*11, 12*). There are limited differences in chromatin accessibility and regulatory histone marks between ISCs and their differentiated descendants despite distinct gene expression profiles (*13, 14*), underscoring the intrinsic plasticity among intestinal cell types that facilitates tissue repair and regeneration. While disruption of stem cell and differentiation programs is observed in CRC, which is the third most common and second most deadly malignancy worldwide (*15*), we have yet to define regulators of cell state plasticity in cancer initiation.

Most sporadic CRCs initiate as a premalignant adenoma harboring genomic alterations that constitutively activate WNT signaling (*16, 17*), most often through loss-of-function *APC* mutations (*18, 19*). A key component of a cytoplasmic destruction complex, adenomatous polyposis coli (APC) restricts WNT signaling by facilitating ubiquitin-mediated degradation of β-catenin (*20–22*). Once APC function is compromised, β-catenin accumulates in the nucleus, where it can operate as the primary effector of aberrant WNT signaling (*23, 24*). ISC expansion and imbalanced crypt-villus homeostasis are known outcomes of *Apc* deletion and constitutive β-catenin activity in mouse models of intestinal neoplasia (*25, 26*). Beyond these cellular outcomes, the nongenetic transcriptional consequences and cell state heterogeneity following deleterious *APC* mutations are poorly understood.

Restoring the expression of functional APC can reinstate WNT pathway regulation and suppress cancer initiation (*27–29*). Inhibiting WNT-dependent Lgr5+ stem cells can impair tumor growth and metastasis (*30, 31*). Translating these concepts into effective therapy

[1]Department of Medical Oncology, Dana-Farber Cancer Institute, Boston, MA, USA. [2]Department of Medicine, Brigham and Women's Hospital and Harvard Medical School, Boston, MA, USA. [3]Broad Institute of Massachusetts Institute of Technology and Harvard University, Cambridge, MA, USA. [4]Department of Gastroenterology, The First Affiliated Hospital of Chongqing Medical University, Chongqing, China. [5]Department of Pathology, Brigham and Women's Hospital and Harvard Medical School, Boston, MA, USA. [6]Division of Gastrointestinal Oncology, Department of Medical Oncology, Dana-Farber Cancer Institute, Boston, MA, USA.
*Corresponding author. Email: nilay_sethi@dfci.harvard.edu
†These authors contributed equally to this work.
‡These authors contributed equally to this work.
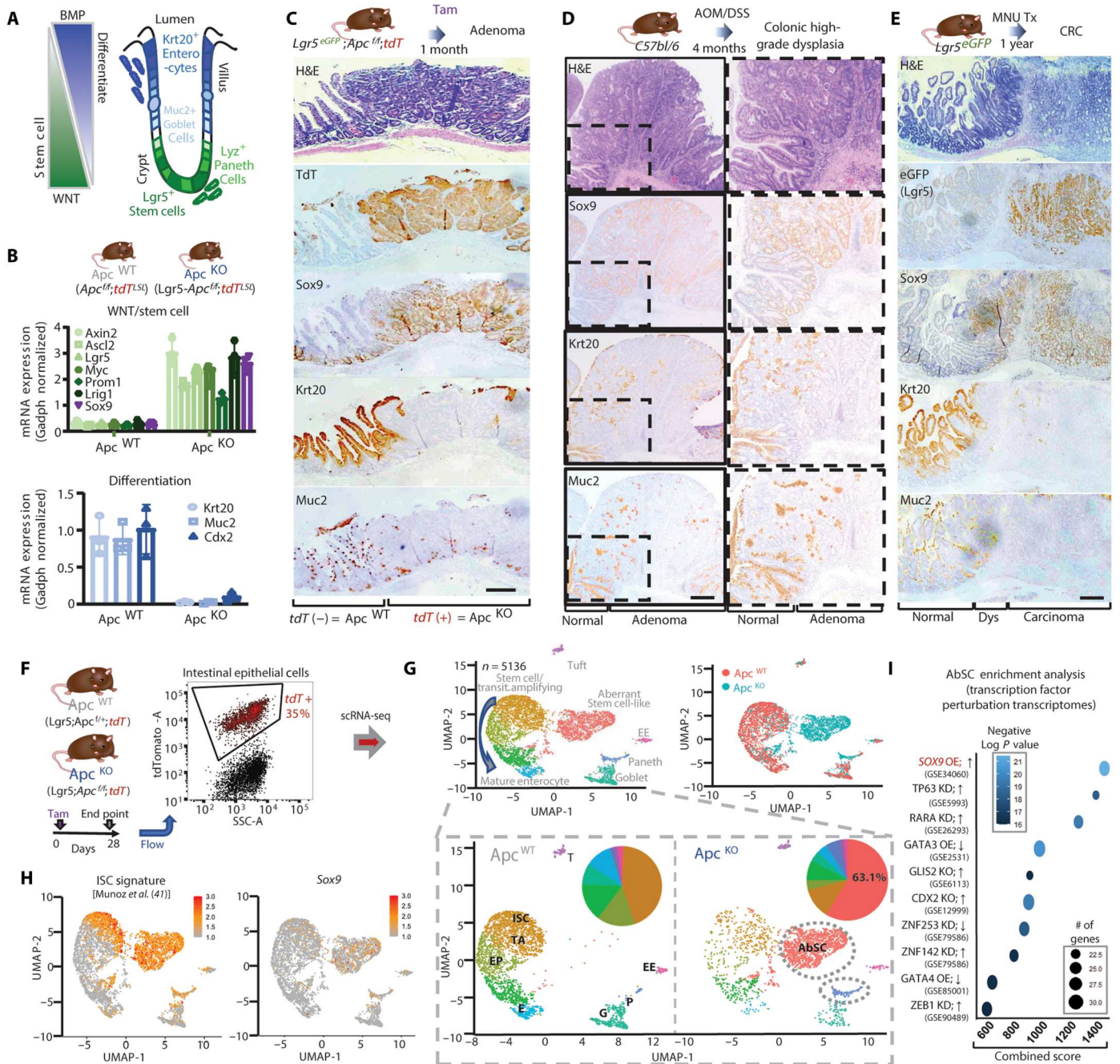
Fig. 1. Impaired differentiation is a conserved mechanism of aberrant cell state plasticity in mouse models of intestinal neoplasia. (**A**) Schematic depicting WNT and BMP signaling gradient in normal intestines. Stem cells and Paneth cells reside in the crypt base, whereas differentiated cell types are in the villus. (**B**) Relative mRNA expression of Wnt/stem cell (top) and differentiation (bottom) genes in intestines of indicated mice by quantitative reverse transcription polymerase chain reaction (qRT-PCR); means ± SD of three biological replicates. (**C**) Representative images of intestinal lesions from $Lgr5^{Cre}$;$Apc^{f/f}$;$R26^{tdT}$ mice including hematoxylin and eosin (H&E) staining and tdTomato (tdT), Sox9, Krt20, and Muc2 IHC. Scale bar, 250 μm. (**D**) Representative images of intestinal lesions from AOM/DSS-treated mice including H&E staining Sox9, Krt20, and Muc2 IHC. Normal and adenoma regions were labeled. Scale bar, 250 μm. (**E**) Representative images of intestinal lesions from MNU-treated Lgr5^{eGFP} mice including H&E staining and eGFP (Lgr5-expressing cells), Sox9, Krt20, and Muc2 IHC. Normal, dysplastic, and carcinoma regions were labeled. Scale bar, 250 μm. (**F**) tdT$^+$ intestinal epithelial cells isolated by fluorescence-activated cell sorting (FACS) from $Lgr5^{Cre}$; Apc$^{f/+}$;$R26^{tdT}$ (control) and $Lgr5^{Cre}$;$Apc^{f/f}$;$R26^{tdT}$ (experimental) mice 28 days following tamoxifen induction. (**G**) Uniform manifold approximation and projection (UMAP) representation of single-cell transcriptome profiling of tdT$^+$ epithelial cells from $Lgr5^{Cre}$; Apc$^{f/+}$;$R26^{tdT}$ (control) and $Lgr5^{Cre}$;$Apc^{f/f}$;$R26^{tdT}$ (experimental) mice colored by cell type (top left) and sample identity (top right). UMAP of separated samples along with pie chart indicating cell type distribution (bottom). TA, transit amplifying; EP, enterocyte progenitor; E, mature enterocyte; G, goblet cell; P, Paneth cell; EE, enteroendocrine; T, tuft cell; AbSC, aberrant stem cell–like. (**H**) UMAP representation of ISC signature (left) (41) and Sox9 (right). (**I**) Transcription factor perturbation gene ontology analysis (Enrichr) of top 100 genes up-regulated in AbSC cluster.

has proven difficult, as WNT pathway inhibitors have not advanced in preclinical and clinical testing (*32*). By defining key mediators that facilitate neoplastic initiation, we may uncover new therapeutic strategies for CRC. Here, we characterize critical early molecular events of intestinal neoplasia using histopathological analyses, single-cell transcriptomics, chromatin accessibility assays, and organoid experiments in distinct mouse models and human specimens, uncovering developmental reprogramming as an important early step that supports aberrant cell state plasticity before cancer formation.

RESULTS

Impaired differentiation is a conserved event in multiple mouse models of intestinal neoplasia

To study the molecular underpinnings of aberrant cell state plasticity, we used two genetically engineered and two carcinogen-induced murine models of intestinal neoplasia. $Lgr5^{eGFP-IRES-CreERT2}$;$Apc^{loxP-exon14-loxP}$ ($Lgr5^{Cre}$;$Apc^{f/f}$) genetically engineered mice develop hundreds of adenomas in the small intestines following tamoxifen-induced conditional deletion of Apc (*33*) in Lgr5$^+$ ISCs (fig. S1, A and B) (*10*, *34*). Compared to controls, adenomas from $Lgr5^{Cre}$;$Apc^{f/f}$ mice displayed elevated mRNA expression of canonical WNT downstream targets (*Axin2* and *Myc*) and stem cell genes (*Ascl2*, *Lgr5*, *Prom1*, and *Lrig1*), including *Sox9* (Fig. 1B), consistent with known biology (*35*, *36*). In contrast, markers of differentiated intestinal cells (e.g., *Cdx2*) of both absorptive (e.g., *Krt20*) and secretory lineages (e.g., *Muc2*) (*37*) were down-regulated in $Lgr5$;$Apc^{f/f}$ intestinal adenomas (Fig. 1B). To validate these findings, we examined another previously published genetically engineered mouse model in which inducible Apc knockdown (KD) with or without mutant K-ras^{G12D} activation in Lgr5$^+$ cells displayed robust formation of colonic adenomas (*27*). In agreement with the $Lgr5^{Cre}$;$Apc^{f/f}$ model, genes associated with stem cell activity were up-regulated, whereas intestinal differentiation genes were suppressed in Apc KD colonic adenomas by bulk RNA sequencing (RNA-seq; fig. S1C). We also analyzed protein expression of Sox9 in early intestinal adenomas from $Lgr5^{Cre}$;$Apc^{f/f}$ mice that were crossed with $R26^{LSL-tdTomato}$ ($R26^{tdT}$ or tdT^{LSL}) mice to label Apc^{KO} cells. Compared to the adjacent normal intestinal epithelium in which Sox9 expression is restricted to the crypt base, tdT$^+$ Apc^{KO} lesions demonstrated elevated expression of Sox9 throughout the lesion, which coincided with the absence of differentiation markers Krt20 and Muc2 (Fig. 1C). These observations suggest that Apc inactivation is sufficient to impair intestinal differentiation and leads to inappropriate Sox9 expression in adenomas.

We next evaluated two mouse models of carcinogen-induced small intestinal and colonic neoplastic lesions to ask whether Sox9 activation and impaired differentiation are universal events in cancer initiation that can be achieved by random mutagenesisin vivo. The first, well-established model consists of exposing mice to the procarcinogen azoxymethane (AOM) and irritant dextran sodium sulfate (DSS) (Methods), which leads to colonic lesions ranging from low-grade dysplasia to intramucosal adenocarcinoma after several months. Consistent with our observations in the $Lgr5^{Cre}$;$Apc^{f/f}$;$R26^{tdT}$ model, high-grade dysplastic colonic lesions demonstrated robust Sox9 overexpression and loss of Krt20$^+$ enterocytes and Muc2$^+$ goblet cells (Fig. 1D and fig. S1D). In the second

model, mice were exposed to drinking water containing *N*-methyl-*N*-nitrosourea (MNU), a potent carcinogen with gastrointestinal tropism, and a subset developed poorly differentiated intestinal carcinomas after 1 year. $Lgr5^{Cre-eGFP}$ mice treated with MNU showed marked up-regulation of Sox9 in premalignant and adenocarcinoma lesions (Fig. 1E and fig. S1E), consistent with an early role in cancer development. Differentiation markers Krt20 and Muc2 were absent in premalignant and adenocarcinoma lesions. Elevated expression of Lgr5 as indicated by enhanced green fluorescent protein (eGFP) immunohistochemistry (IHC) was found in intestinal adenocarcinomas but not their associated premalignant lesions, underscoring the central importance of stem cell activation in progression to malignancy (Fig. 1E). These results implicate impaired differentiation and Sox9 activation as a common pathway to CRC initiation.

To characterize the transcriptional program enabling impaired differentiation, we performed single-cell RNA-seq (scRNA-seq) on the $Lgr5^{Cre}$;$Apc^{f/f}$;$R26^{tdT}$ genetic model. tdT$^+$ epithelial cells were isolated from $Lgr5^{Cre}$;$Apc^{f/+}$;$R26^{tdT}$ (controls that are phenotypically wild type) and $Lgr5^{Cre}$;$Apc^{f/f}$;$R26^{tdT}$ mice by fluorescence-activated cell sorting (FACS) 28 days following tamoxifen induction (Fig. 1F). Unsupervised clustering followed by uniform manifold approximation and projection (UMAP) representation of single-cell gene expression profiles revealed that control Apc^{WT} cells displayed the expected distribution of cell lineages based on intestinal markers (fig. S2, A to C) (*38*). In contrast, Apc inactivation led to a fourfold enrichment in Paneth cells (5.9% versus 1.5%) and the emergence of cells that exhibited a new transcriptional state (63.1% versus 0%) at the expense of normal ISCs and differentiated cell types, including absorptive progenitors, mature enterocytes, goblet cells, and, to a lesser extent, enteroendocrine cells (Fig. 1G). tdT$^+$ Apc^{KO} intestinal lesions demonstrated a greater number of Paneth cells by Lyz IHC (fig. S3A), which can also be found at earlier time points of Apc inactivation (*35*, *39*). Apc deletion led to a greater percentage of Lgr5$^+$ cells as indicated by eGFP FACS (fig. S2D), suggesting that ISC activity is up-regulated in Apc^{KO} cells, agreeing with a vast literature (*40*) and supported by the enrichment of published ISC signatures (table S1, Fig. 1H, and fig. S2A) (*38*, *41*). A deeper evaluation revealed that select canonical ISC markers were not consistently found in Apc^{KO} cells, including *Olfm4* (fig. S3, B and C). In contrast, Apc^{KO} cells expressed higher levels of *Sox9* compared to normal ISC (Fig. 1H), which was supported by universal Sox9 expression in tdT$^+$ intestinal lesions from $Lgr5^{Cre}$;$Apc^{f/f}$;$R26^{tdT}$ mice (Fig. 1C). Furthermore, evaluating transcription factor perturbation gene sets that were enriched among up-regulated genes in Apc^{KO} cells (table S1) revealed that a Sox9 overexpression transcriptional program scored the strongest [Fig. 1I (adjusted $P = 3.26 \times 10^{-22}$) and table S2]. These observations suggest that Apc deletion leads to a new transcriptional state with selective ISC transcriptional activity.
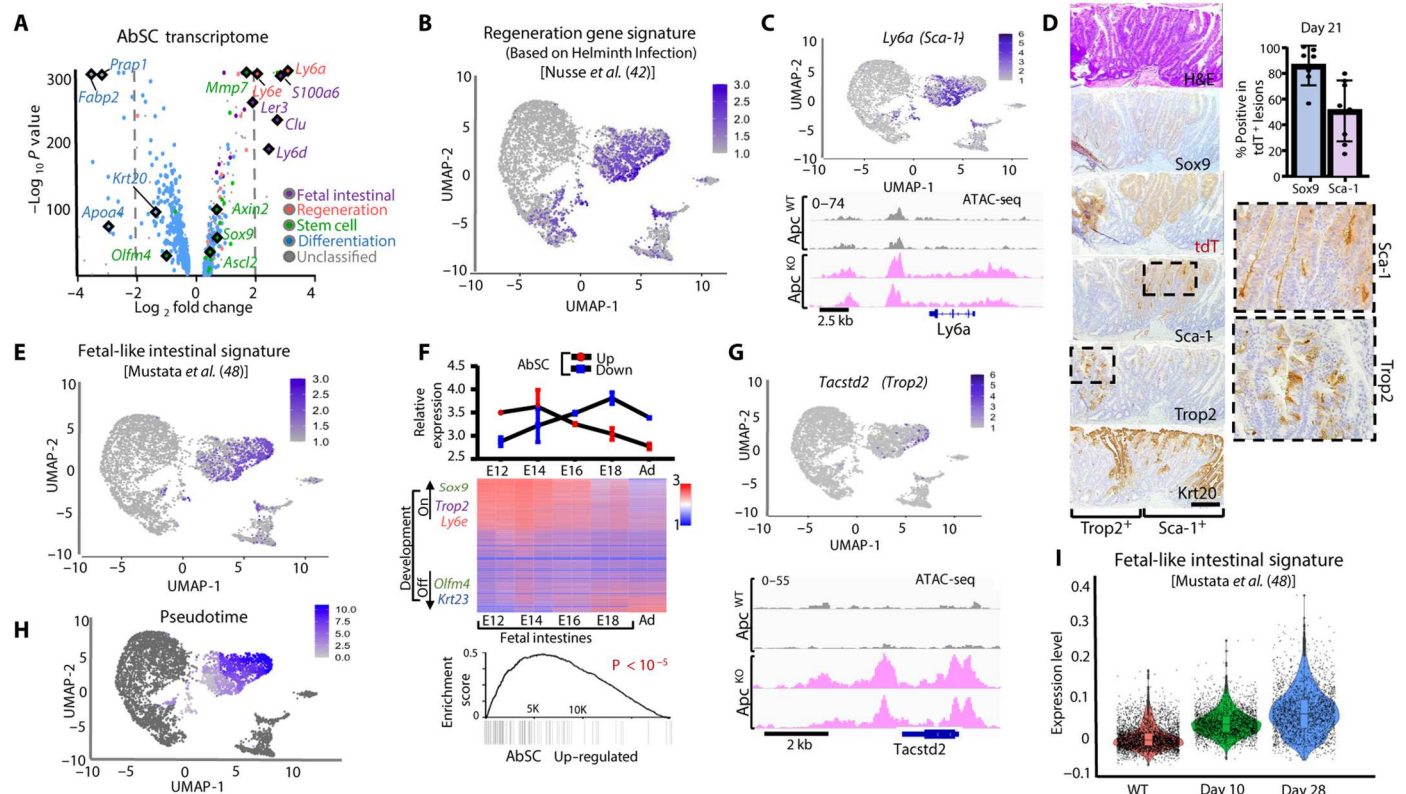
Reactivation of genes associated with fetal intestines upon Apc loss

Despite showing enrichment of most canonical ISC genes, the transcriptional profile of Apc^{KO} cells was found in one distinct cluster (Fig. 1G), expressing genes not found in normal intestinal cells; we, therefore, refer to these cells as aberrant stem cell–like (AbSC). To characterize the AbSC transcriptional program in greater depth, searching for features that explain its distinguished gene expression

profile, we examined the differentially expressed genes in the AbSC cluster relative to all other intestinal clusters. Consistent with our previous results, genes associated with differentiated enterocytes (blue) were down-regulated, whereas ISC markers and WNT pathway targets (green) were up-regulated (Fig. 2A). Genes associated with interferon (IFN) signaling (fig. S4, A and B) were significantly up-regulated in AbSCs, which matched gene ontology analyses implicating IFN pathways and transcription factors (e.g., RELA and nuclear factor κB; fig. S4C and table S2). Genes associated with regeneration (pink) and fetal intestines (purple) were also uniquely and significantly up-regulated in the AbSC cluster (Fig. 2A). A regeneration gene expression signature derived from an experimental intestinal helminth infection model [Nusse *et al.* (*42*); table S1] was specifically up-regulated in AbSCs (Fig. 2B). Notably, this gene expression signature is also associated with IFN-γ signaling, indicating a potential link between regeneration and IFN-γ signaling (*42*).

Among regeneration genes within AbSCs, *Ly6a* and *Ly6e* consistently showed the strongest and most abundant expression (Fig. 2C

and fig. S4D). While Apc inactivation led to minor overall chromatin accessibility changes at regeneration genes (fig. S4E), there was greater access at *Ly6a* and *Ly6e* genomic loci by assay for transposase accessible-chromatin (ATAC-seq; Fig. 2C and fig. S4D) (*43*). We decided to focus on *Ly6a* [also referred to as stem cell antigen-1 (Sca-1)] as a marker for validation studies because of its (i) selective high-level expression in a substantial fraction of AbSC cells (63.1%), (ii) absence from normal intestinal clusters, and (iii) association with stem cell properties in the hematopoietic system (*44*–*46*). Greater chromatin accessibility at the *Ly6a* genomic locus upon Apc deletion corresponded to elevated *Ly6a* mRNA expression by reverse transcription polymerase chain reaction (RT-PCR; fig. S4F). $Lgr5^{Cre};Apc^{f/f};R26^{tdT}$ mice displayed selective Sca-1 expression in tdT$^+$ intestinal lesions and, within these lesions, Sca-1 was expressed in 30 to 40% of tdT$^+$ cells (Fig. 2D). Sca-1$^+$ cells also expressed Sox9, which was found in approximately 85% of tdT$^+$ cells (Fig. 2D) but did not consistently express Lgr5/eGFP or Olfm4 (fig. S4, G and H). To examine self-renewal properties of Sca-1$^+$ AbSCs, we performed organoid-forming assays using tdT$^+$

Fig. 2. Reactivation of genes associated with fetal intestinal development upon *Apc* inactivation. (**A**) Volcano plot showing differentially expressed genes from AbSC cluster. Enterocyte (blue), stem cell (green), regeneration (salmon), and fetal intestine (purple) genes are highlighted. (**B**) Normalized regeneration gene signature expression (*42*) on UMAP plot. (**C**) Normalized *Ly6a* expression on UMAP plot (top). Chromatin accessibility at *Ly6a* genomic locus in tdT$^+$ cells isolated by FACS from *Lgr5*-tdT and *Lgr5*-Apc$^{f/f}$-tdT mice by ATAC-seq (bottom). (**D**) Representative images of intestinal lesions from *Lgr5*-Apc$^{f/f}$-tdT mice including H&E staining and tdTomato (tdT), Sca-1 (quantification on top right), Trop2, and Krt20 IHC. Scale bar, 250 μm. (**E**) Normalized fetal-like intestinal gene signature expression (*48*) on UMAP plot. (**F**) Average expression of differentially up-regulated (red) and down-regulated (blue) genes across fetal intestines at indicated time points of mouse development by RNA-seq (*1*). Heatmap representing differentially expressed genes in embryonic day 12 (E12) fetal intestines compared to adult intestines ranked by fold change; a normalized enrichment score of up-regulated genes in AbSC is shown on the right ($P < 1 \times 10^{-5}$). Ad, adult. (**G**) Normalized *Tacstd2* expression on UMAP plot (top). Chromatin accessibility at *Tacstd2* genomic locus in tdT$^+$ cells isolated by FACS from *Lgr5*-tdT and *Lgr5*-Apc$^{f/f}$-tdT mice by ATAC-seq (bottom). (**H**) Pseudotime analysis of AbSCs using Monocle 3. (**I**) Violin plot indicated expression of fetal-like intestinal gene signature expression (*48*) in tdT$^+$ intestinal cells from *Lgr5*-tdT control and *Lgr5*-Apc$^{f/f}$-tdT at day 10 and 28 following tamoxifen induction. *P* value calculated by Wilcoxon rank sum test with Bonferroni correction.

cells isolated by FACS. Consistent with in situ observations, ~28% of tdT$^+$ cells from $Lgr5^{Cre}$;$Apc^{f/f}$;$R26^{tdT}$ mice demonstrated Sca-1 protein expression by FACS, whereas tdT$^+$ cells from $Lgr5$-tdT mice showed no expression (fig. S4I). Per 1000 cells plated, Sca-1$^+$ cells showed a 7.4-fold greater organoid-forming ability than Sca-1$^-$ cells isolated from $Lgr5^{Cre}$;$Apc^{f/f}$;$R26^{tdT}$ mice (fig. S4, J and K). Dissociated Sca-1$^+$ organoids passaged into secondary cultures maintained a 5.9-fold greater organoid forming ability than Sca-1$^-$ cells (fig. S4L), suggesting population stability and preserved regenerative properties. These data suggest that sustained regenerative transcriptional activity is a feature of neoplastic initiation and contributes to self-renewal capacity.

Fetal intestinal genes were also up-regulated in AbSCs (Fig. 2A). Consistently, two relatively nonoverlapping fetal-like gene signatures [Vallone *et al.* (*47*) and Mustata *et al.* (*48*); table S1] mapped specifically to the AbSC cluster (Fig. 2E and fig. S5, A and B). To confirm these associations, we also interrogated bulk gene expression data directly extracted from intestines at different stages of embryonic development (*1*). AbSC down-regulated genes had stronger expression in late development [embryonic day 18 (E18)] and adult intestines compared to earlier stages of intestinal development (Fig. 2F, E12 to E16). By contrast, AbSC upregulated genes are significantly enriched among genes preferentially expressed in embryonic relative to adult intestines (Fig. 2F), which include *Sox9*, *Tacstd2* (encoding Trop2), and *Ly6e*. Among fetal intestinal genes, *Tacstd2* showed the most specific expression in AbSCs, marking at least 11% of the cluster (Fig. 2G), which was confirmed by Trop2 IHC in intestinal lesions from the genetic mouse model (Fig. 2D). While greater chromatin accessibility was found at fetal genes upon Apc inactivation (fig. S5C), new accessibility was observed at the *Tacstd2* genomic locus (Fig. 2G). These analyses suggest that expanded cell state plasticity by gaining access to and transcriptionally activating fetal intestinal genes is associated with intestinal neoplasia.

Regenerative and fetal-intestinal gene signatures appeared to occupy distinct compartments of the AbSC cluster, which was confirmed by a coexpression analysis of *Tacstd2* and *Ly6a* (fig. S5D), higher resolution reclustering of AbSCs (fig. S5E), and relative nonoverlapping Sca-1 and Trop2 IHC in tdT$^+$ intestinal lesions (Fig 2D). Pseudotime analysis of AbSCs indicated that gene expression associated with regeneration preceded that of fetal intestines (Fig. 2H). To examine this possibility, we performed scRNA-seq on tdT$^+$ cells isolated from $Lgr5^{Cre}$;$Apc^{f/f}$;$R26^{tdT}$ mouse intestines 10 days following tamoxifen-induction (fig. S5F). As expected, AbSC activity was significantly elevated 10 and 28 days following Apc inactivation (fig. S5G). While *Ly6a* expression was stably elevated at days 10 and 28 (fig. S5H), fetal intestinal gene expression, including *Tacstd2*, gradually increased over time (Fig. 2I and fig. S5I), consistent with regeneration preceding developmental reprogramming. These data also suggest that nongenetic factors are responsible for fetal gene activation following regenerative transcriptional activity.

Carcinogen-induced colon neoplasia demonstrates developmental reprogramming

To define features of AbSC in an independent model of colon neoplasia, we performed scRNA-seq of a neoplastic lesion and paired a normal sample from a mouse exposed to AOM/DSS. UMAP representation of single-cell gene expression profiles of epithelial cells revealed known cell types in the normal colon and a distinct transcriptional profile in the colonic lesion (Fig. 3A). AbSC gene signature derived from our genetic model demonstrated the strongest expression in a neoplastic cluster furthest from normal tissue profiles and weaker expression in the remaining neoplastic cells and normal ISCs (Fig. 3B). Neoplastic cells demonstrated greater *Ly6a* expression by scRNA-seq (fig. S6A) and Sca-1 staining by IHC, the latter of which showed specific expression in lesions without expression in adjacent or distal normal tissue (Fig. 3E and fig. S6B). Notably, expression of the fetal intestinal gene signature broadly (Fig. 3C) and *Tacstd2* specifically (Fig. 3D and fig. S6C) was restricted to neoplastic cells. Consistent with these results, strong Trop2 expression was only found in premalignant and malignant lesions (Fig. 3E), corresponding to elevated Sox9 expression and attenuation of differentiation markers. These results demonstrate that a carcinogen-induced colon neoplasia model demonstrates developmental reprogramming in neoplastic cells, particularly marked by Trop2 positivity.

To validate and extend these findings, we analyzed a recently published bulk RNA-seq dataset derived from AOM/DSS-treated mice at four different time points of colon neoplastic evolution (*49*) (Fig. 3F). Compared to untreated controls, transcriptional profiles of colonic lesions showed enhanced stem cell activity and impaired differentiation over time (fig. S6, D and E). Colonic lesions at week 10, the latest time point evaluated, showed significant enrichment of regeneration and fetal intestinal gene signatures compared to untreated controls (Fig. 3, G and H). The regeneration program peaked at week 2 and then gradually declined over time (Fig. 3, G and I). In contrast, the fetal intestinal gene signature gradually increased over time, showing the strongest levels at week 10 (Fig. 3, H and I). These transcriptional program kinetics are consistent with histopathological evaluation of colonic lesions from our AOM/DSS model, which demonstrated robust Sca-1 expression in early compared to more advanced lesions, whereas Trop2$^+$ expression followed the opposite pattern, with stronger staining in more advanced lesions compared to early ones (fig. S7). Furthermore, these results corroborate those found in our genetic model (Fig. 2, H and I), whereby developmental reprogramming lags behind regeneration activity in neoplastic progression (Fig. 3I).

Human familial adenomatous polyposis adenoma and derivative organoids display impaired differentiation and AbSC activity

To evaluate transcriptional abnormalities in human CRC initiation, we evaluated adenoma and paired normal from a 39-year-old patient with familial adenomatous polyposis (FAP), a hereditary condition in which a mutant copy of *APC* is inherited, hundreds to thousands of intestinal adenomas develop, and prophylactic colectomy is required to prevent progression to cancer (*50*). In agreement with our mouse models, colon adenomas displayed elevated expression of SOX9 and TROP2 compared to adjacent normal tissue (Fig. 4A). Markers of differentiated absorptive and secretory colonic cells were partially suppressed as shown by KRT20 and MUC2 IHC, respectively (Fig. 4A). This observation could reflect limited WNT pathway restriction due to hypomorphic mutant APC activity (*51*) or admixture of normal colonic tissue.

We next performed scRNA-seq on cryopreserved adenoma and paired normal tissue. UMAP representation of single-cell gene expression profiles revealed four epithelial clusters derived from
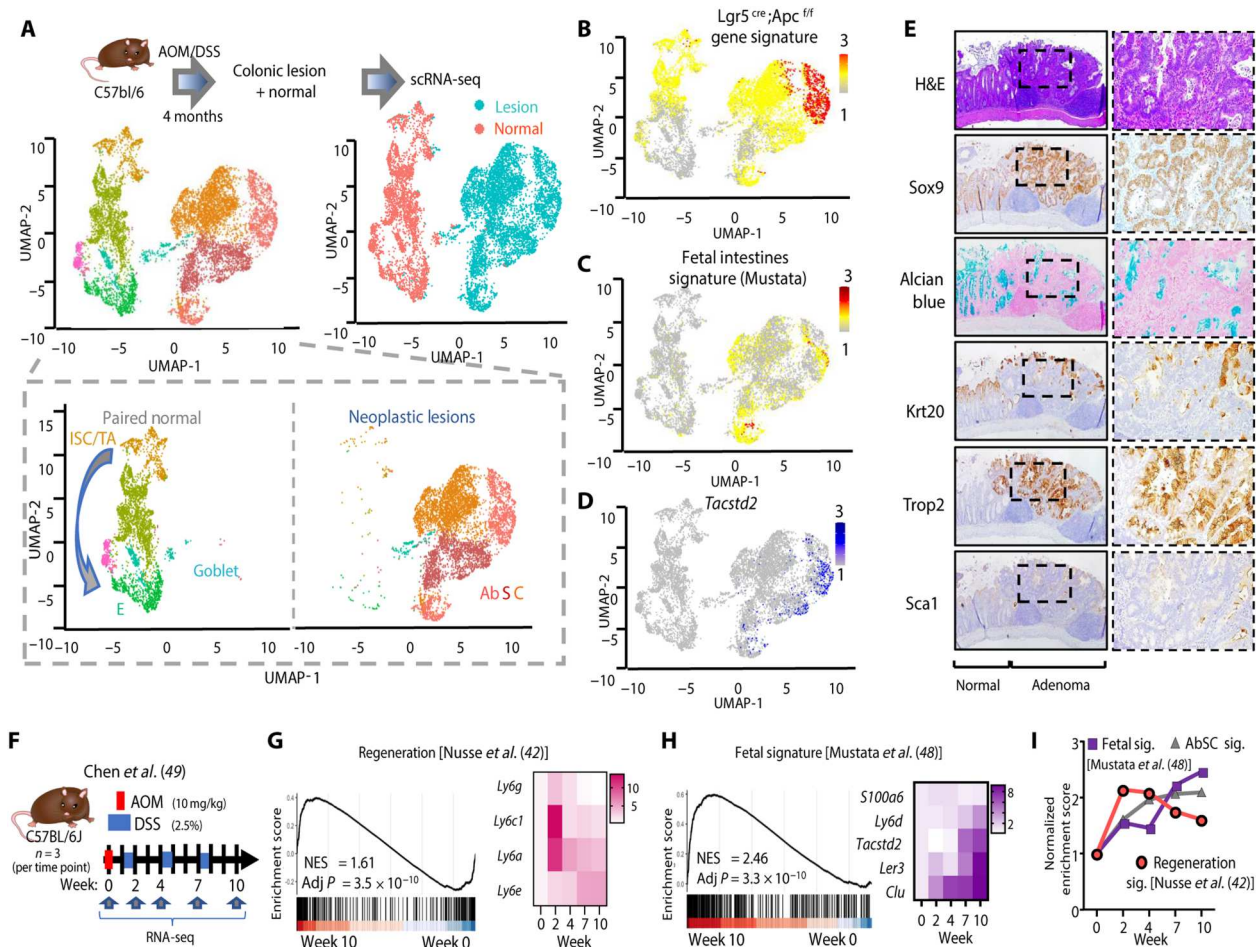
Fig. 3. scRNA-seq of carcinogen-induced model of colonic neoplasia demonstrates developmental reprogramming. (**A**) UMAP plot of epithelial cells from a colon lesion and adjacent normal epithelium of an AOM/DSS-treated mouse model of colon carcinogenesis, colored by cell type (top left) and origin (top right). UMAPs from lesions and normal are separately depicted (bottom). TA, transit amplifying; E, mature enterocyte. (**B**) Feature plot of Lgr5;Apc[KO] gene signature on AOM/DSS UMAP. (**C**) Feature plot of fetal-like gene signature (*48*) on AOM/DSS UMAP. (**D**) Feature plot of *Tacstd2* (Trop2) expression on UMAP. (**E**) Representative images of a high-grade dysplastic colonic lesion from an AOM/DSS-treated mouse including H&E and Alcian blue (AB) staining, as well as Sox9, Krt20, Sca-1, and Trop2 IHC. (**F**) Experimental workflow for AOM/DSS induced colonic tumor model (GSE178145) (*49*). Bulk RNA-seq of three biological replicates at indicated time points was analyzed. (**G**) Gene set enrichment analysis (GSEA) of regeneration gene signature (*42*) on AOM/DSS lesions at week 10 versus controls (left) and heatmap of associated genes over time (right) (*49*). (**H**) GSEA of fetal-like intestinal gene signature (left) (*48*) on AOM/DSS lesions at week 10 versus controls (left) and heatmap of associated genes over time (right) (*49*). (**I**) Normalized enrichment scores for regeneration gene signature, fetal-like intestinal gene signature, and AbSC gene signature over time in AOM/DSS data from (*49*).

adenoma and normal tissue (Fig. 4B and fig. S8A); however, unlike our mouse models and consistent with human histopathology, the separation between adenomatous and normal tissue was less distinct. To define these clusters, we first used established gene signatures to identify normal enterocyte and goblet cell clusters (Fig. 4, B and C, and fig. S8 B to D). We then defined the cluster found only in the adenoma sample as "Aberrant" (Fig. 4B). The remaining cluster was labeled "Intermediate" because (i) it was found in both normal and adenoma tissue and (ii) it did not engender a normal cell type gene expression profile (Fig. 4B) (*38*). Reassuringly, SOX9 expression was highest in the Aberrant cluster followed by the Intermediate cluster, whereas KRT20 expression was lowest in these two clusters (Fig. 4C and fig. S8C). In general, the expression of ISC signatures was greatest in the Aberrant cluster relative to Intermediate, enterocyte, and goblet clusters (figs. S9A and S8E), further building confidence in our classification. Notably, the AbSC gene expression

signature was greatest in the Aberrant cluster and adenoma tissue (Fig. 4D and fig. S8F). A subset of regeneration and fetal-like intestinal signatures and genes, including *TACSTD2*, were elevated in the Aberrant cluster (figs. S9B and S8, G and H). We validated these findings using published scRNA-seq data from patients with CRC (*n* = 9) using normal colon (*n* = 3) as a comparator (fig. S10, A to E). Together, these data indicate that human adenomas demonstrate a partial block in differentiation and activation of an AbSC program involving developmental programs.

We next evaluated organoids derived from adenoma and normal colonic tissue from the same patient with FAP, asking whether features of AbSC activity are captured in this three-dimensional culture system that requires supplemented WNT3A, R-spondin, and Noggin (WRN) conditioned media rich in stem cell promoting factors (*52*). Normal colonic cultures contained organoids that appeared folded by phase contrast and generated crypts with high
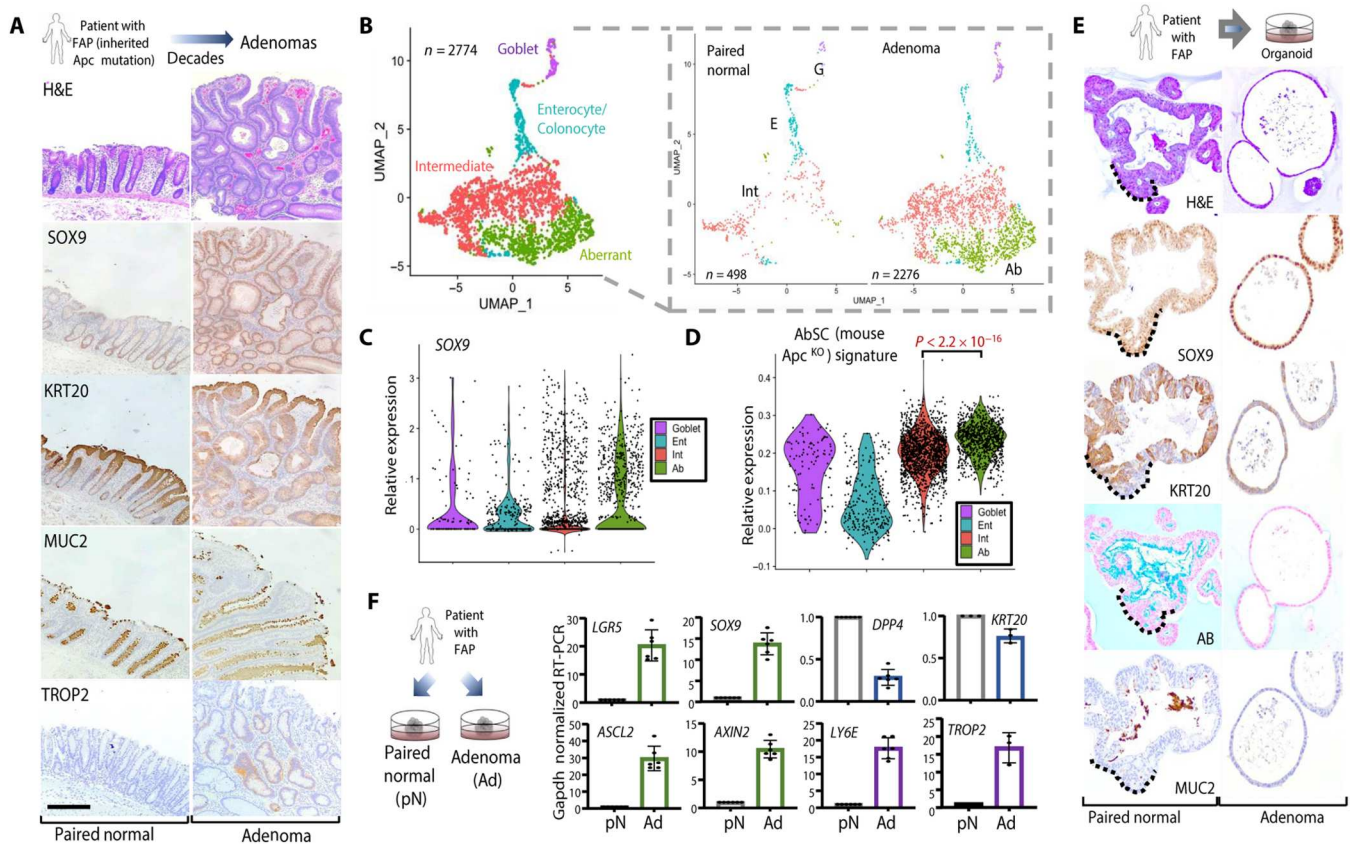
Fig. 4. Characterization of human FAP adenomas by histopathology and scRNA-seq. (**A**) Representative images of adenoma and normal adjacent colon tissue from patient with FAP including H&E staining SOX9, KRT20, and MUC2 IHC. Scale bars, 250 μm. (**B**) UMAP representation of scRNA-seq of human adenoma and paired normal indicating four distinct cell clusters; E, enterocyte; Int, intermediate; Ab, aberrant; G, Goblet. (**C**) Violin plot indicated *SOX9* expression in four different cell clusters. (**D**) Violin plot indicated the expression of the AbSC gene signature in four different cell clusters. *P* value calculated by Wilcoxon rank sum test with Bonferroni correction. (**E**) Representative images of organoids derived from adenoma and adjacent-normal tissue from patient with FAP including H&E and AB staining Sox9, Krt20, and Muc2 IHC; the dotted line in the paired normal sample indicates one of several crypts in the organoid. (**F**) mRNA expression of *SOX9*, stem cell marker *LGR5*, WNT pathway markers *AXIN2* and *ASCL2*, AbSC markers *LY6E* and *TROP2*, and intestinal differentiation markers *KRT20* and *DPP4* in FAP organoids by qRT-PCR. Data are expressed as means ± SD of three biological and two technical replicates.

SOX9 expression, absent KRT20 expression, and absent MUC2 expression/Alcian blue (AB) staining (Fig. 4E, dotted line). These organoids also displayed differentiated regions with low or no SOX9 expression, high KRT20 expression, intermittent MUC2 expression, and strong AB staining (Fig. 4E). In contrast, most organoids in adenomas cultures (>95%) did not display differentiated regions as indicated by unfolded, spheroid morphology by phase contrast and weak KRT20 levels and absent MUC2 expression by IHC. Rather, adenoma organoids expressed uniform high SOX9 levels (Fig. 4E). These findings were confirmed in a broader survey of stem cell/WNT (*LGR5*, *SOX9*, *ASCL2*, and *AXIN2*) and regeneration/developmental genes (*LY6E* and *TACSTD2*), which demonstrated markedly higher mRNA expression in adenoma compared to normal organoid cultures (Fig. 4F). *Ly6a* was not profiled, as it does not have a direct human homolog. mRNA expression of colonic differentiation markers *DPP4* and *KRT20* were correspondingly reduced, albeit modestly because of enhanced stem cell cues conferred by WRN media (Fig. 4F).

We validated these results in Apc^WT and Apc^KO organoids derived from our genetic mouse model (fig. S9, C to E). After

confirming Apc inactivation in tdT^+ organoids conferred niche independence (the ability to grow without WRN media; fig. S9D), we performed bulk RNA-seq. In addition to the activation of stem cell genes and partial reduction in intestinal differentiation, Apc^KO organoids demonstrated robust activation of developmental intestinal genes, especially *Tacstd2* (fig. S9E). Collectively, these data suggest that human adenoma and mouse Apc^KO organoids display features of developmental reprogramming as part of an AbSC transcriptional program.

Sox9 is required for intestinal neoplasia initiation

On the basis of its (i) enriched transcriptional activity in AbSCs, (ii) stronger expression in fetal intestines compared to adult intestines, and (iii) ability to functionally block differentiation in models of CRC (*9*), we hypothesized that Sox9 is required for CRC initiation. To evaluate this hypothesis, we bred *Lgr5^Cre*;*Apc^f/f*;*R26^tdT* mice with *Sox9^f/f* mice (*53*) to homozygosity, enabling conditional biallelic deletion of Sox9 in the Apc^KO setting upon tamoxifen induction. Experiments were initiated with three daily tamoxifen injections followed by weekly single-injection maintenance treatments, attempting to force robust genetic recombination. Successful Sox9

inactivation prevented tdT⁺ adenoma formation, reduced mRNA levels of stem cell genes (*Ascl2* and *Lgr5*), and maintained intestinal homeostasis with crypt-restricted Lgr5^{eGFP+} stem cells and Krt20⁺ differentiated villi (Fig. 5A). While *Lgr5^{Cre};Apc$^{f/f}$;Sox9$^{f/f}$;R26^{tdT}* mice survived significantly longer than *Lgr5^{Cre};Apc$^{f/f}$;R26^{tdT}* controls (Fig. 5B), they eventually succumbed to adenoma burden. These adenomas invariably expressed Sox9 despite tdT⁺ activation and Apc deletion, suggesting escape of Sox9 deletion, which we confirmed by PCR of flow-sorted tdT⁺ cells, demonstrating a significant fraction of unrecombined Sox9 (fig. S11A). To show that tdT⁺ adenomas from *Lgr5^{Cre};Apc$^{f/f}$;Sox9$^{f/f}$;R26^{tdT}* mice were still dependent on Sox9, we generated organoids at the experimental end point and subjected them to ex vivo recombination using specific adenovirus (Ad) infections. Compared to organoids treated with mock Ad^{GFP} controls, Ad$^{GFP-Cre}$-treated organoids displayed reduced proliferation by CellTiter-Glo (CTG), which corresponded to robust Sox9 inactivation by recombination-specific PCR (Fig. 5C). We confirmed these results by performing a 10-day short-term experiment, isolating organoids from three mice from each genotype, and subjecting them to Ad$^{GFP-Cre}$ infections followed by CTG (fig. S11B). Collectively, these experiments indicate that successful Sox9 inactivation prevents intestinal Apc^{KO} adenomas using genetically engineered mice and derivative organoids.

We next established colon organoids without endogenous Cre recombinase for controlled ex vivo Ad$^{GFP-Cre}$ experiments, seeking further validation of Sox9 dependency in colonic adenomas. Colon organoids from *R26^{tdT}*, *Apc$^{f/f}$;R26^{tdT}*, and *Apc$^{f/f}$;Sox9$^{f/f}$;R26^{tdT}* mice were infected with Ad$^{GFP-Cre}$ and subjected to proliferation assays by CTG. While Apc inactivation led to a 7.5-fold increase in organoid proliferation, concomitant Sox9 deletion reduced this proliferative advantage by threefold (Fig. 5D). To support these findings, we performed tdT⁺ quantification by FACS as a surrogate for cell viability following Ad$^{GFP-Cre}$ treatment. tdT was activated in 54% of *Apc$^{f/f}$;R26^{tdT}* organoids 4 days after Ad$^{GFP-Cre}$ infection, which was reduced by fourfold to 13% in *Apc$^{f/f}$;Sox9$^{f/f}$;R26^{tdT}* organoids (fig. S11C); similar results were achieved with lentiviral Cre activation (fig. S11D). Last, compared to Ad^{GFP}-treated controls, Ad$^{GFP-Cre}$ treated *Apc$^{f/f}$;Sox9$^{f/f}$;R26^{tdT}* organoids demonstrated impaired proliferation by Ki67 IHC, which was not observed in *R26^{tdT}* or *Apc$^{f/f}$;R26^{tdT}* organoids (Fig. 5E and fig. S11E).
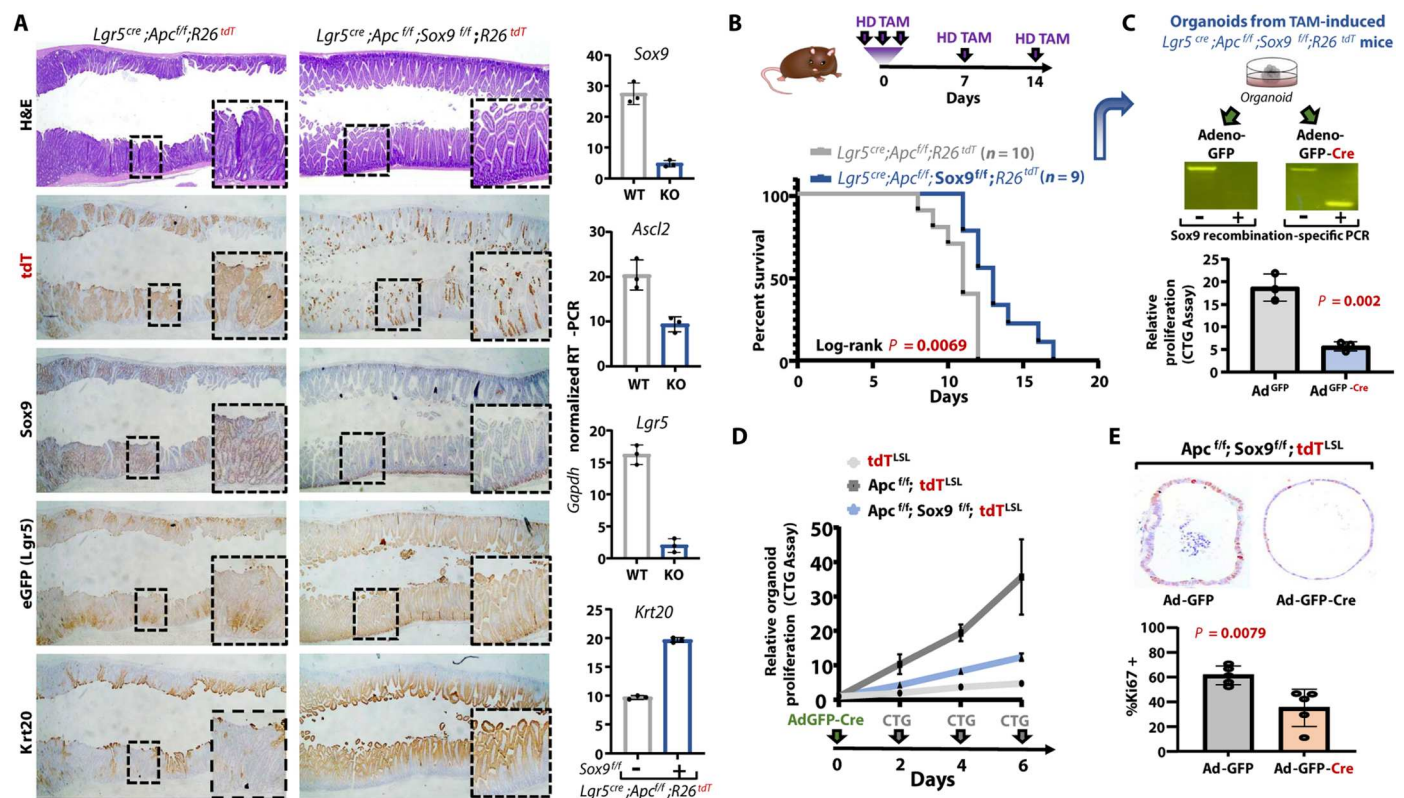
Fig. 5. Sox9 is required for Apc^{KO} adenomas and organoids. (**A**) Representative images of H&E staining and tdT, Sox9, Lgr5(eGFP), and Krt20 IHC from *Lgr5*-Apc$^{f/f}$-tdT (control) and *Lgr5*-Apc$^{f/f}$-Sox9$^{f/f}$-tdT (experimental) mice small intestine; corresponding normalized mRNA expression of *Sox9*, *Ascl2*, *Lgr5*, and *Krt20*. Data are expressed as means ± SD of three biological replicates. (**B**) Schematic of in vivo experimental design. Kaplan-Meier survival curve of *Lgr5*-Apc$^{f/f}$-tdT (*n* = 10) and *Lgr5*-Apc$^{f/f}$-Sox9$^{f/f}$-tdT (*n* = 9) mice using high-dose (HD) tamoxifen (TAM) for induction and maintenance. Log-rank *P* = 0.0069. (**C**) Organoids from *Lgr5*-Apc$^{f/f}$-Sox9$^{f/f}$-tdT mice were generated at the experimental endpoint, treated with either Ad^{GFP} or Ad$^{GFP-Cre,}$ and subjected to *Sox9* recombination-specific PCR and a proliferation assay by CTG. Data are expressed as means ± SD of three biological replicates. *P* values were calculated by a two-sided Student's *t* test. (**D**) Proliferation of organoids derived from tdT, Apc$^{f/f}$-tdT, and Apc$^{f/f}$-Sox9$^{f/f}$-tdT mice and infected with Ad$^{GFP-Cre}$ at indicated time points by CTG. Data are expressed as means ± SD of three biological replicates. (**E**) Organoids derived from tdT, Apc$^{f/f}$-tdT, and Apc$^{f/f}$-Sox9$^{f/f}$-tdT mice were infected with Ad^{GFP} or Ad$^{GFP-Cre}$, formalin-fixed, and then processed for histopathology. Representative images of Ki67 IHC. Quantification of %Ki67 positivity in five to six organoids per condition. *P* values were calculated by two-sided Student's *t* test. WT, wild type; KO, knockout.

$Apc^{f/f};Sox9^{f/f};R26^{tdT}$ organoids with more efficient Ad$^{GFP-Cre}$ infection marked by increased tdT activation demonstrated reduced Sox9 expression and lower proportion of Ki67$^+$ cells relative to poorly infected ones (fig. S11E, red versus gray arrow). These experiments demonstrate a requirement for Sox9 in adenoma formation using genetically engineered mice and organoids.

scRNA-seq reveals that Sox9 is required for AbSC

To determine whether Sox9 is required for AbSC transcriptional activity, we performed scRNA-seq on FACS-isolated tdT$^+$ cells from $Lgr5^{Cre};Apc^{f/f};Sox9^{f/+};R26^{tdT}$ mice 1 month after tamoxifen induction. We chose $Lgr5^{Cre};Apc^{f/f};Sox9^{f/+};R26^{tdT}$ mice to analyze tdT$^+$ cells with consistent and reliable reduction in Sox9 expression given our difficulty in isolating viable tdT$^+$ cells with efficient homozygous deletion of Sox9 (Fig. 5, B and C). Reassuringly, viable tdT$^+$ cells from $Lgr5^{Cre};Apc^{f/f};Sox9^{f/+};R26^{tdT}$ mice demonstrated a considerable reduction in Sox9 levels compared to $Lgr5^{Cre};Apc^{f/f};R26^{tdT}$ mice, which displayed higher Sox9 expression relative to $Lgr5^{Cre};R26^{tdT}$ controls (Fig. 6A and fig. S12, A and B). UMAP representation of single-cell gene expression profiles revealed clusters representing the normal epithelial cell types and AbSCs (Fig. 6A and fig. S12C). Notably, single copy deletion of Sox9 reduced the percentage of AbSCs from 60 to 10% in tdT$^+$ Lgr5-Apc^{KO} cells (Fig. 6A and table S3) and significantly reduced

AbSC gene signature activity (Fig. 6B), indicating a requirement for Sox9 in maintaining an AbSC transcriptional program. ISC gene signatures were also reduced in tdT$^+$ cells from $Lgr5^{Cre};Apc^{f/f};Sox9^{f/+};R26^{tdT}$ mice (Fig. 6B and fig. S12, D and E). The sixfold reduction in AbSC cells was accompanied by the restoration of a normal distribution of ISC and differentiated intestinal cell types (Fig. 6A and table S3). We also observed reduced expression of IFN-γ, regeneration signatures, including $Ly6a$, and fetal-like intestinal gene signatures, including $Tacstd2$, in tdT$^+$ cells from $Lgr5^{Cre};Apc^{f/f};Sox9^{f/+};R26^{tdT}$ mice (fig. S11, F to K). These results were confirmed in $R26^{tdT}$, $Apc^{f/f};R26^{tdT}$, and $Apc^{f/f};Sox9^{f/f};R26^{tdT}$ organoids using ex vivo Ad$^{GFP-Cre}$ infections followed by RT-PCR (fig. S13). ATAC-seq profiling revealed that Sox9 inactivation led to reduced chromatin accessibility at regeneration and fetal genes in Apc^{KO} cells (Fig. 6C and fig. S14A), specifically at the $Ly6a$, $Ly6e$, and $Tacstd2$ genomic loci (Fig. 6D and fig. S14B), indicating rescue of expanded cell state plasticity. Collectively, these results demonstrate a requirement of Sox9 in AbSC activity, aberrant cell state plasticity, and fetal intestinal gene reactivation.

SOX9 KD in FAP adenoma organoid induces differentiation

To evaluate SOX9 activity and necessity in human colonic neoplasia, we used our FAP adenoma organoid model (Fig. 4E). We first defined genomic SOX9 binding patterns in paired normal colon
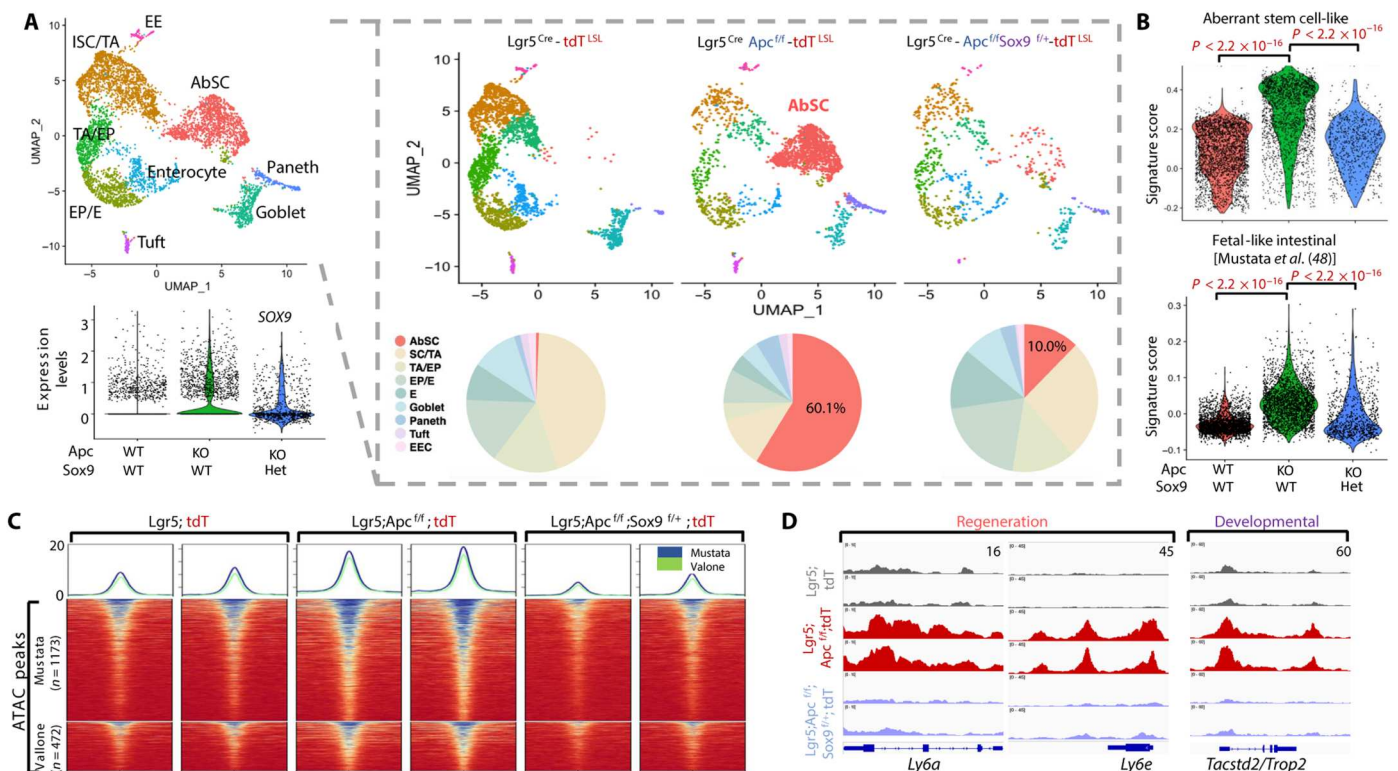

Fig. 6. Sox9 suppression restricts AbSC and developmental reprogramming by scRNA-seq. (**A**) UMAP representation of scRNA-seq data from tdT$^+$ cells isolated by FACS from $Lgr5$-tdT, $Lgr5$-Apc$^{f/f}$-tdT, and $Lgr5$-Apc$^{f/f}$-Sox9$^{f/+}$-tdT mice a month after tamoxifen induction colored by clusters and then separated by sample. Violin plot of normalized single-cell Sox9 expression in each group. Pie charts indicating the distribution of clusters in each sample. SC, stem cell; TA, transient amplifying; E, enterocyte; EEC, enteroendocrine cell. (**B**) Violin plot of normalized expression of AbSC gene signature (top) and fetal-like intestines gene signature (bottom) (48) in each group. P value calculated by Wilcoxon rank sum test with Bonferroni correction. (**C**) Heatmap depicting chromatin accessibility at fetal genes from two published signatures (42, 48) in tdT$^+$ cells flow-sorted from the intestines of $Lgr5$-tdT ($n = 2$), $Lgr5$-Apc$^{f/f}$-tdT ($n = 2$), and $Lgr5$-Apc$^{f/f}$-Sox9$^{f/+}$-tdT ($n = 2$) mice. (**D**) Integrative genomics viewer screenshots depicting chromatin accessibility at $Ly6a$, $Ly6e$, and $Tacstd2$ genomic loci in tdT$^+$ cells flow-sorted from the intestines of $Lgr5$-tdT, $Lgr5$-Apc$^{f/f}$-tdT, and $Lgr5$-Apc$^{f/f}$-Sox9$^{f/+}$-tdT mice.

and adenoma organoids by cleavage under targets and release under nuclease (CUT&RUN). A global increase in SOX9 binding was observed in adenoma organoids compared to normal colon organoids (fig. S15A). Greater SOX9 binding was observed at ISC and AbSC genes in adenoma compared to normal colon organoids (Fig. 7A and fig. S15B); while many sites are shared, there appears to be greater than fourfold unique SOX9 binding sites at AbSC genes in adenoma compared to normal (Fig. 7B), although the data are limited to one biological replicate. Consistent with selective ISC activity upon Apc inactivation, we noticed that SOX9 binding at ISC gene *LRIG1* was unchanged in adenoma compared to normal colon organoids (fig. S15C), whereas greater SOX9 binding was found at a *PROM1* intronic enhancer (fig. S15C), validating our previous work (*9*) and supporting SOX9-mediated AbSC activity in neoplasia. We also found greater SOX9 binding at both Mustata and Vallone fetal genes, as well as Nusse regenerative genes in adenoma compared to

normal colon organoids (Fig. 7, B and C, and fig. S15, D to F). A total of 213 AbSC and 108 fetal genes were only bound by SOX9 in adenoma organoids (table S6). Consistently, stronger SOX9 binding was found at fetal genes, including *TACSTD2* and *CLU*, in adenoma compared to normal colon organoids (Fig. 7D). Despite the enrichment in adenoma organoids, we think that there is considerably more SOX9 binding at fetal genes in normal colon organoids than expected, likely because of strong and sustained influences of WRN conditioned media.

We next asked whether SOX9 is required for AbSC activity in human FAP adenoma organoids. Human adenoma organoid cultures showed few differentiating organoids (~5%), which appear as folded structures by phase contrast, whereas organoid cultures derived from normal adjacent tissue displayed evidence of a differentiating population that amounted to about 50% by day 3 (Fig. 7E and fig. S16A). Using this system, we examined whether short
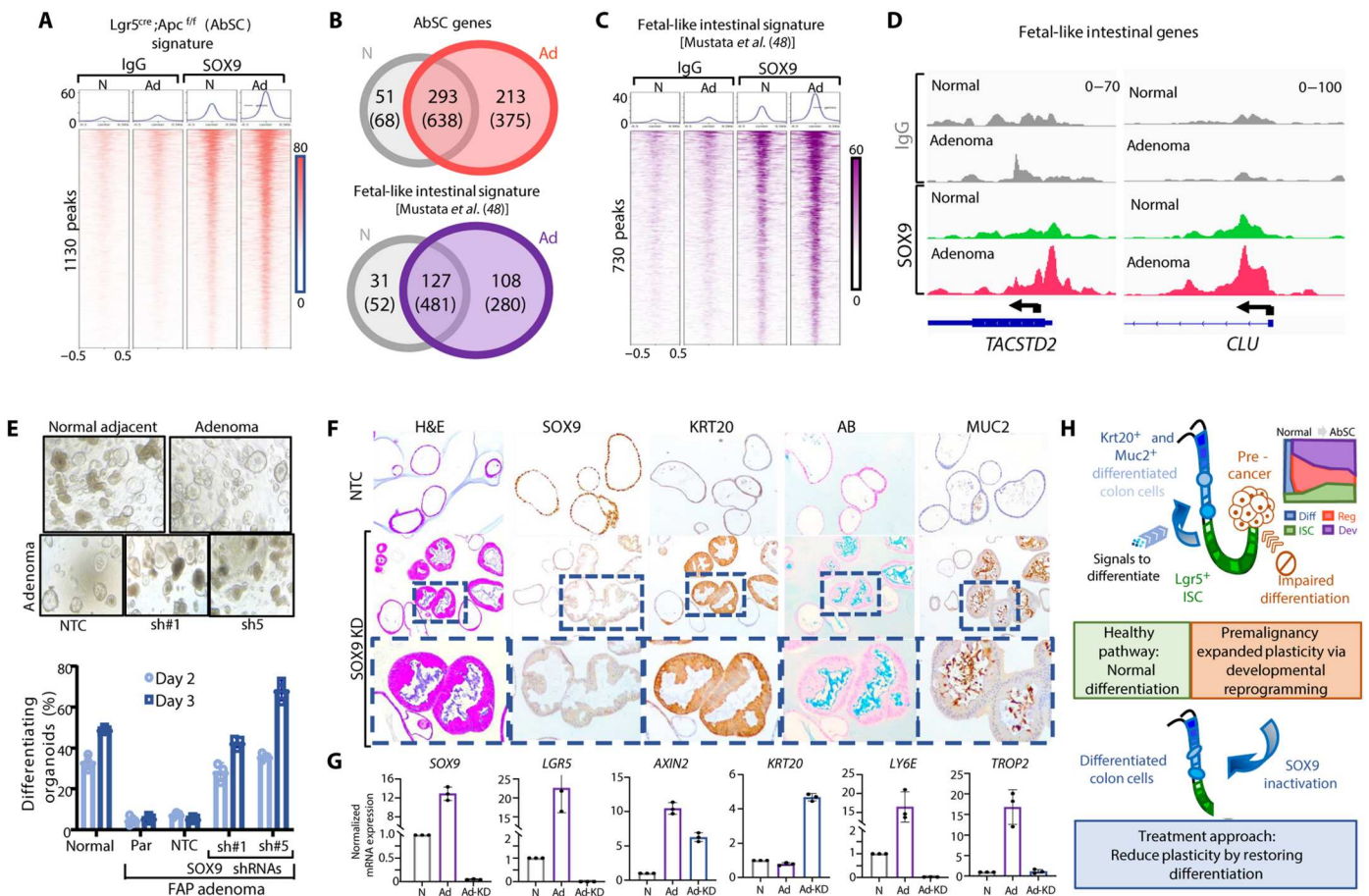
Fig. 7. SOX9 KD impairs fetal reprogramming and induces differentiation in FAP adenoma organoids. (**A**) Heatmap of SOX9 binding associated with AbSC genes (1130 peaks) in normal colon (*n* = 4 technical replicates) and adenoma (*n* = 4 technical replicates) organoids from a patient with FAP by CUT&RUN. (**B**) Venn diagram of high-confidence SOX9 bound genes (peaks) using log fold change ≥ 0.5 compared to immunoglobulin G (IgG) control in normal colon and adenoma organoids for genes in AbSC (top) and fetal-like intestines (bottom) (*48*). (**C**) Heatmap of SOX9 binding associated with fetal-like intestinal (730 peaks) (*48*) in normal colon and adenoma organoids by CUT&RUN. (**D**) SOX9 binding at fetal intestinal genes *TACSTD2* and *CLU* in normal colon and adenoma organoids by CUT&RUN. (**E**) Phase contrast images depicting differentiation phenotype (folded) of organoids derived from normal colon and adenoma organoid cultures (top row); adenoma organoids expressing NTC or two distinct shRNAs against SOX9 (bottom row). Quantification of differentiating organoids in indicated cultures at days 2 and 3; Par, parental. (**F**) Representative images of H&E; AB staining; and SOX9, KRT20, and MUC2 IHC of NTC and SOX KD FAP adenoma organoids. (**G**) Normalized mRNA expression of *SOX9*, *LGR5*, *AXIN2*, *KRT20*, *LY6E*, and *TROP2* in indicated organoids: normal adjacent mucosa (N), adenoma-NTC (Ad), and adenoma-SOX9 KD (Ad-KD). (**H**) Schematic summarizing AbSC transcriptional program and developmental reprogramming obstructing intestinal differentiation in CRC initiation and the ability of SOX9 suppression to reverse these effects.

hairpin RNA (shRNA)–mediated SOX9 KD can force differentiation in human adenoma organoids. Stable SOX9 KD shifted the adenoma culture to 40 to 70% differentiating organoids, representing up to a 14-fold increase compared to parental and nontargeting control (NTC) cultures by day 3 (Fig. 7E and fig. S16, B and C). Histopathology of fixed organoids demonstrated that SOX9 KD induced robust KRT20 expression by IHC and mucin production by AB staining and MUC2 IHC (Fig. 7F). Consistently, SOX9 KD reduced stem cell activity (*LGR5*, *SOX9*, and *AXIN2*) and regenerative/developmental reprogramming (*LY6E* and *TROP2*) while inducing differentiation (*KRT20*; Fig. 7G). In contrast, SOX9 KD led to a modest, statistically insignificant increase in differentiation of normal colon organoids, which corresponded to induction of KRT20 without impact on fetal genes (fig. S16, D and E). These data indicate that human FAP adenomas depend on SOX9 to maintain developmental reprogramming and prevent differentiation (Fig. 7H).

DISCUSSION

Our study indicates that reactivation of a fetal intestinal program is a critical component of an aberrant transcriptional state that restricts differentiation and expands cell state plasticity during CRC initiation. *APC* is the most frequently mutated gene in CRC (*19*). In the intestines, *Apc* inactivation leads to unrestricted WNT activity and ISC expansion, which contribute to adenoma formation. However, whether WNT activation by APC loss of function leads to normal ISC transcriptional activity could not be resolved using previous methods. By applying scRNA-seq to an Apc^KO genetic mouse model, we found that Apc inactivation leads to a transcriptional cell state with distinguished features compared to normal ISCs; we therefore refer to this program as an aberrant rather than a hyperactive stem cell–like state. While up-regulation of the WNT pathway and ISC activity is part of the AbSC program, these alone do not capture the complete cadre of deviant consequences following Apc inactivation. A unique transcriptional program that consists of inappropriate IFN-related signaling, sustained regeneration, and re-engagement of developing fetal intestinal genes was found in a subset of Apc^KO intestinal epithelial cells. There appears to be a convergence of two of these transcriptional programs on *Ly6a*, which has been shown to be a target of IFN signaling in pathological states in the intestines such as colitis (*54*) and infection (*42*), as well as implicated in epithelial regeneration following injury (*55*) or stem cell ablation (*42, 56*). Regenerative transcriptional activity is transient during pathological states, such as infection, and expression of fetal genes is temporally restricted during development. However, expression of these programs following Apc inactivation is sustained and may have consequences that permit neoplastic progression. It appears that persistent regeneration activity precedes and may enable the emergence of developmental gene expression. In agreement with these results, open chromatin was found at regenerative genes in line with the potential need to express these programs with prompt kinetics, whereas new accessibility was associated with fetal genes, potentially explaining its delayed expression following Apc inactivation.

Reactivation of genes that operate during fetal development has been observed in CRC (*57*) and other cancers (*58, 59*); however, our data indicate that the reactivation of developmental genes can be traced to premalignant disease before malignant transformation.

Identification of fetal genes that are consistently activated in premalignant colonic lesions, therefore, carry significant diagnostic value, as their expression would normally be silenced in adult tissue under homeostatic conditions; the difficulty may arise in the specificity of such a diagnostic marker if transiently expressed during infectious, inflammatory, or other non-neoplastic pathologic states. Carcinoembryonic antigen, better known as CEA, is a CRC biomarker that has proven useful in perioperative and disease recurrence settings (*60, 61*). Accessing silenced regions of the genome that were once active during pluripotent development would intuitively serve the faculty of expanding cell state plasticity and adaptive fitness among other advantageous properties for neoplastic growth (*62*) and metastasis (*63*). Developmental reprogramming is a nongenetic feature that would confer clonal fitness through epigenetic inheritance. Defining the precise functional importance of aberrant cell state plasticity in cancer (*6*) and fetal intestinal program reactivation in CRC initiation (*57*) will require deeper characterization.

One unifying consequence of the aberrant transcriptional state involves impaired intestinal differentiation, although our experiments do not necessarily distinguish between blocked differentiation and de-differentiation, two often indistinguishable mechanisms leading to expanded cell state plasticity (*6*). Because the intestine is the most rapidly renewing epithelium in the human body, any genomic alteration or transcriptional state that promotes neoplasia must counteract the natural tissue turnover. A mutation that does not promote intestinal tissue fixation is unlikely to have neoplastic consequences, at least during cancer initiation. Beyond genetic mouse models that delete or suppress *Apc*, random mutagenesis leads to premalignant and malignant lesions with a similar molecular pattern of impaired differentiation. Adenomas from a patient with an inherited *APC* mutation demonstrated attenuation of intestinal differentiation rather than a complete block. There is evidence that adenomas in patients with FAP select for *APC* mutations that retain partial function, which is postulated to confer optimal β-catenin activity to facilitate cancer initiation (*64*). In agreement with these genomic findings, biochemical reconstruction of the destruction complex demonstrated that truncated APC mutants are functional hypomorphs that retain limited WNT restricting capacity (*51*), likely explaining their ability to partially obstruct differentiation, impart clonal fitness, and yield insidious neoplastic benefits.

Given that preventing differentiation is a hallmark of CRC initiation, the translational question is whether restoring or inducing differentiation can serve as a therapeutic strategy, one that has proven successful for a subset of leukemias (*6, 65*). The proof of concept of this strategy for CRC lies in studies that reintroduced functional APC and demonstrated restoration of regulated WNT signaling, induction of intestinal differentiation, and inhibition of cancer growth (*27–29*). Furthermore, disrupting WNT-dependent stem cell programs by eliminating Lgr5+ stem cells (*30, 31*) or ectopically expressing prodifferentiation transcription factors such as HOXA5 (*66*) impaired tumor growth and metastasis in preclinical models. Translating these important studies into effective therapeutics remains the challenge. One possibility is that interfering with normal ISC activity is insufficient, given the additional aberrant faculties endowed by Apc inactivation. SOX9 not only is important for adult crypt biology and ISC activity but also appears to be a critical driver of the AbSC state. Sox9 was previously shown to be required for intestinal regeneration, a component of the AbSC

transcriptional program, following radiation injury (*67*). Compromised Apc function led to elevated Sox9 expression, which may approach levels of Sox9 found in fetal intestinal development (*1*) and enable the reactivation of developmental genes through pioneering activity (*68*), especially in the setting of greater chromatin accessibility. SOX9 may therefore serve as a better target than other ISC drivers, as disrupting its activity will also interfere with aberrant developmental reprogramming. Genetic inactivation of *Sox9* in our mouse model and suppression in human FAP adenomas reduces not only ISC gene signatures but also fetal intestinal transcriptional programs. Beyond preventing adenoma formation, SOX9 suppression also disrupts the growth of established neoplastic murine organoids and human cancers by inducing intestinal differentiation (*9*). Hence, SOX9 is required for cancer initiation and maintenance; it can therefore be targeted as a preventative strategy in hereditary polyposis syndromes and as a treatment approach in sporadic CRC.

Study limitations

While we demonstrate that transcriptional activity associated with regeneration precedes fetal gene expression in a population of Apc^KO intestinal cells, we did not demonstrate whether this occurred in a single-cell lineage, which would require individual cell tracking (e.g., barcoding). We provide a potential reason underlying the partial impairment of differentiation in human adenomas from a patient with FAP; however, additional experiments are required to prove that this observation is due to hypomorphic mutant APC activity. While Cre expression from the endogenous *Lgr5* locus leads to efficient inactivation of Apc, a positively selected alteration, it appears less proficient for inactivating both copies of Sox9, a negatively selected event. Future efforts should use a stronger Cre driver to more efficiently delete Sox9 in vivo. Our CUT&RUN data indicate that SOX9 binds to several regeneration and fetal genes in adenoma organoids; however, these results are limited by (i) a single biological replicate and (ii) the influence of WRN media, which is a potent inducer of a stem cell state. Direct tissue evaluation and/or evaluation of organoids grown in factor-reduced media across multiple biological replicates will provide stronger evidence that SOX9 directly regulates fetal reprogramming.

METHODS

Animal studies

All procedures involving mice and experimental protocols were approved by the Institutional Animal Care and Use Committee (IACUC) of Dana-Farber Cancer Institute (11-009). Adenoma and paired normal-appearing tissue from a patient with FAP were collected after colectomy with informed consent under approval (protocol 13-189) by the Internal Review Board of the Dana-Farber Cancer Institute, Boston, MA, USA.

The generation of *Lgr5*^eGFP-IRES-CreERT2 mouse was described earlier (*69*). *Lgr5*^eGFP-IRES-CreERT2 mice were backcrossed in C57bL/6J mice and subsequently single-nucleotide polymorphism (SNP)–tested to ensure >97% pure background (Taconic). To inactivate Apc in intestinal tissue, we crossed Apc^f/f mice (a gift from C. Perret) to *Lgr5*^eGFP-IRES-CreERT2. These mice were further crossed to *R26*-LSL-tdTomato purchased from the Jackson Laboratory (JAX, stock #007905) (*70*) for conditional tdT labeling of Lgr5^+ stem cells and their progeny. To delete Sox9, mice were crossed to Sox9^flox mice (JAX, stock #013106) (*53*).

To activate conditional alleles, experimental mice aged 6 to 8 weeks were injected intraperitoneally with a single-dose tamoxifen (50 μl of sunflower oil at 10 mg/ml) unless otherwise indicated. For MNU model, *Lgr5*^eGFP-IRES-CreERT2 mice were treated with drinking water containing 240 parts per million of MNU (bioKEMIX) scheduled every other week for 10 weeks and followed for 1 year. For AOM/DSS model, AOM/DSS treatment was performed as previously described (*71*). Briefly, at 8 to10 weeks of age, mice were injected intraperitoneally with AOM (10 mg/kg; Sigma-Aldrich) and treated with 2% DSS (30 to 50 kDa; colitis grade; MP Biomedicals) in drinking water for 5 days. DSS treatment was repeated three times once per 4 weeks. Mice were euthanized 11 weeks after AOM injection.

Mice were euthanized at the end point of the experiment, and small intestine and colon were removed from mice, flushed with phosphate-buffered saline (PBS), and incubated in 10% formalin for 5 min. Subsequently, intestines were opened longitudinally, "Swiss-rolled," incubated overnight in 10% formalin at room temperature, and processed for paraffin embedding. Fresh tissue was collected for organoid generation, RNA isolation, and protein collection and flash-frozen for long-term storage.

Human specimen

Adenoma and paired normal-appearing tissue from a patient with FAP were collected after colectomy under approval (protocol 13-189) by the Internal Review Board of the Dana-Farber Cancer Institute, Boston, MA, USA.

Histopathology

Paraffin-embedded intestines, organoids, or xenograft tumors were serially sectioned and mounted on a slide. Sections were subjected to hematoxylin and eosin (H&E), AB–periodic acid–Schiff (AB-PAS), as well as immunostaining, using standard procedures. For morphological analysis, sections were serially dehydrated in xylene and ethanol and stained with H&E for histological assessment or AB-PAS to identify goblet cells and mucus.

Immunofluorescence and IHC

For immunostaining, antigen retrieval was performed using a sodium citrate buffer (pH 6), Trilogy (Sigma-Aldrich Cell Marque), or tris-EDTA (pH 9). Slides were permeabilized using a 0.2% Triton X-100 for 30 min at room temperature and blocked with donkey serum for 1 hour. The primary antibodies used for IHC were rabbit anti-Sox9 [1:600; Cell Signaling Technology (CST), #82630; Trilogy antigen retrieval], rabbit anti-Mucin2 (1:200; Santa Cruz Biotechnology, sc-15334; tris-EDTA), anti-Krt20 (1:500; CST, #13063; tris-EDTA), anti–red fluorescent protein [RFP; 1:500; Rockland, 600-401-379; sodium citrate (pH 6)], anti-eGFP (1:1000; Abcam, ab290; tris-EDTA), anti-Olfm4 [1:1000; CST, #39141; sodium citrate (pH 6)], anti-Lyz, anti–Sca-1/Ly6a [1:150; Abcam, ab109211; sodium citrate (pH 6)], anti-Axin2 [1:800; Abcam, ab32197; sodium citrate (pH 6)], and rabbit anti-Ki67 [1:1000; CST, #12202; sodium citrate (pH 6)]. The binding of primary antibody was detected with 3,39-diamino-benzidine-tetrahydrochloride-dihydrate and counterstained with hematoxylin.

IHC quantification was performed using Fiji Is Just Image J (FIJI) application on 10× images from a Leica DM750 microscope. Ly6a- or Sox9-positive cells were quantified and expressed as a

percentage of total tdT$^+$ cells in intestinal lesions. For organoids, the percentage of Ki67-positive cells was quantified and expressed as a percentage of total cells in an organoid.

Flow analysis, sorting, and staining

Isolated intestines from euthanized mice were washed with ice-cold PBS; villi were scraped using glass slides and dissociated in 5 mM EDTA in PBS at 4°C for 20 min, shaking every 5 to 7 min for about 30 s. The epithelial fraction was collected by centrifugation and incubated at 37°C for 30 min in prewarmed 4× TrypLE. Single cells were filtered through a 70-μm filter after trypsinization, washed with complete media, and collected in FACS buffer.

For antibody staining, 100 μl of resuspended cells in FACS buffer were incubated with 1 μl of APC-labeled Sca-1 antibody (Thermo Fisher scientific, catalog no. 17-5981-82) for 20 min on ice, washed with PBS, and collected in FACS buffer. Cells were resuspended in 1 to 2 ml of FACS buffer with 4′,6-diamidino-2-phenylindole, passed through another 70-μm filter before transferring to 40-μm filtered FACS tubes and sorted. Sorted cells were collected in 5 ml of 50% fetal bovine serum (FBS) + 50% Dulbecco's modified Eagle medium (DMEM) complete with 10 μM Y27632 Rho-kinase inhibitor.

Single-cell RNA-seq

Murine intestines and human adenoma samples were processed as described above and then subjected to scRNA-seq with or without cell hashing. If hashed, then the mouse cells were stained with Total-Seq-30301 Hashtag 1 (BioLegend, #155861) and TotalSeq-30302 Hashtag 2 (BioLegend, #155863) antibodies; no hashing was used for human samples. Viable cells were washed and resuspended in PBS with 0.04% bovine serum albumin at a cell concentration of 1000 cells/μl. About 17,000 viable mouse cells were loaded onto a 10x Genomics Chromium instrument (10x Genomics) according to the manufacturer's recommendations. The scRNA-seq libraries were processed using Chromium single-cell 5′ library and gel bead kit (10x Genomics). Matched cell hashing libraries were prepared using a single-cell 5′ feature barcode library kit. Quality controls for amplified cDNA libraries, cell hashing libraries, and final sequencing libraries were performed using Bioanalyzer High Sensitivity DNA Kit (Agilent). The sequencing libraries for scRNA-seq were normalized to 4 nM concentration and pooled using a volume ratio of 4:1. The pooled sequencing libraries were sequenced on Illumina NovaSeq S4 300 cycle platform. The sequencing parameters were as follows: read 1 of 150 base pairs (bp), read 2 of 150 bp, and index 1 of 8 bp. The sequencing data were demultiplexed and aligned to mm10-3.0.0 using Cell Ranger version 3.1.0 pipeline (10x Genomics).

scRNA-seq analysis

Preprocessing, alignment, and gene counts

Demultiplexing, alignment to the transcriptome, and unique molecular identifier collapsing were performed using the Cell Ranger toolkit provided by 10x Genomics.

General clustering

Standard procedures for quality control filtering, data scaling and normalization, detection of highly variable genes, and hashtag oligo (HTO) demultiplexing were followed using the Seurat v3 in RStudio. Cells with unique feature counts lower than 100 and greater than 25,000 and cells with greater than 25% mitochondrial DNA were excluded. Counts were log-normalized and scaled by a factor of 10,000 according to the default parameters when using the Seurat LogNormalize function. Variable features were identified, and the data were scaled using the default parameters (Ngenes = 2000) of the FindVariableFeatures FIG and ScaleData Seurat functions, respectively. HTOs were demultiplexed using the HTODemux function, and cells were identified as containing HTO-1 or HTO-2 based on their maximal HTO-ID signal. The cell population was filtered to contain only HTO-positive, singlet cells for further analysis. Principle components analysis (PCA) was completed on the remaining cells, and 10 principal components were selected for clustering, t-distributed stochastic neighbor embedding, and UMAP analyses. Cells were visualized primarily using UMAP nonlinear dimensional reduction (dimensions, 1:10; resolution = 0.3), from which feature plots were generated to demonstrate distribution of gene expression and APC^{WT} versus APC^{KO} cells and expression levels of various marker genes throughout the population. Marker genes for each resulting cluster were found using the FindMarkers function with the minimum prevalence set to 25%. One cluster was determined to be immune cells based on top marker genes and excluded from further analysis. Cluster identities were defined using known marker genes for intestinal epithelial cell types. For AOM/DSS model and human FAP samples, immune, stromal, and other supporting cell types were removed to focus the analysis on epithelial cells.

General analysis

scRNA-seq IntegrateData function in Seuratv4 was used to counteract batch effects among human tissue (paired normal A, paired normal B, and adenoma) and mouse model samples. PCA was then completed on the integrated object, and the number of principal components selected for clustering was determined using the integrated object's elbow plot. Cells were then visualized primarily using UMAP nonlinear dimensional reduction from which feature and violin plots were generated to demonstrate the distribution of gene expression and expression levels of various marker genes and gene signatures throughout the population.

scRNA-seq gene signature analysis

To analyze existing gene signatures on our scRNA-seq data, the Seurat AddModuleScore function in Seurat v4 was used to calculate the average normalized and scaled gene expression of a given gene list in each individual cell. Specific cell types were identified using established marker genes and gene signatures (38). Gene signature scoring was then visualized with feature and violin plots. To generate novel gene signatures, the Seurat FindMarkers function was used to create lists of genes differentially expressed in one specified subset in comparison to another given subset. The minimum prevalence was set to 25%.

Pseudotime analysis

After Seurat processing, single-cell transcriptomic profiles of the cells belonging to the AbSC cluster were fitted with a principal graph using the learn_graph() function in Monocle3. By assuming that the earliest cells would most resemble the wild-type ISCs, we ordered these cells along the learned graph whereby the earliest cells have the highest expression of ISC gene signatures.

Assay for transposase-accessible chromatin sequencing

ATAC libraries were prepared as described previously (72). Briefly, flow-sorted tdT$^+$ cells (25,000 cells in duplicates) were lysed to prepare nuclear pellets, which then underwent transposition with TDE1 Enzyme (Illumina, 20034197). Tagmented DNA was purified

using Zymo DNA Clean and Concentrator-5 Kit (catalog no. D4014), and the purified DNA was PCR-amplified with NEBNext 2X Master Mix and Illumina adapters (table S4). The libraries were purified after PCR using AMPure XP beads (Beckman Coulter). 150-bp paired-end reads were sequenced on a NovaSeq instrument (Illumina).

ATAC data processing
ATAC-seq data were analyzed as described previously (PMID: 28648363). Briefly, reads were mapped to the mm10/GRCm38 genome using Bowtie2 aligner version 2.3.5 (72). MACS2 was used to call peaks using the parameters "-t $bamfile -f BAMPE -n qc/macs/$base.macs2 -q 0.01 -g mm" (73). Bigwig files were generated using deepTools bamCoverage with the options "bamCoverage --binSize 10 --smoothLength 30 -p 4 --normalize using RPGC --effectiveGenomeSize 2730871774 --extendReads $fragLength -b $file -of bigwig" (PMID: 24799436). All bigwig and bed files were filtered using the ENCODE Blacklist. Only peaks with $P < 0.00001$ were considered for further analyses. Proximal peaks (−2 kb to 2 kb relative to transcription start site (TSS) called by MACS2 were linked/annotated to genes by ChIPseeker version 1.34.1 (74). Then, computeMatrix and plotHeatmap functions from deepTools (75) were used to visualize peaks.

CUT&RUN sequencing
CUT&RUN for SOX9 and immunoglobulin G (IgG) control in adenoma and normal organoids was done using CUTANA ChIC/CUT&RUN kit (Epicypher, #14-1048) following the manufacturer's protocol. Briefly, 5×10^5 cells were captured with concanavalin A, permeabilized using 0.01% digitonin, and incubated with 0.5 µg of antibody [anti-Sox9 (CST, #82630) and IgG (Epicypher, #13-0042)] in 50 µl of antibody buffer [20 mM Hepes at pH 7.5, 150 mM NaCl, 0.5 mM spermidine, 1× protease inhibitor cocktails (EDTA-free tablet; Roche), 2 mM EDTA, and 0.01% digitonin] overnight. After removing unbound antibody, pAG-MNase (20×) in 50 µl of cell permeabilization buffer was added to the cells and incubated for 10 min at room temperature. Then, $CaCl_2$ (2 mM) was added to activate MNase and incubated at 4°C for 2 hours. The reaction was stopped using 33 µl of 2× STOP buffer and *Escherichia coli* spike-in DNA (0.5 ng) was added as a control. The DNA from the released chromatin in the supernatant was purified and then quantified using Qubit dsDNA HS assay kit (Agilent Technologies). CUT&RUN libraries were constructed using a NEBNext Ultra II DNA library preparation kit as described previously (73) with a few modifications. Briefly, end repair and dA-tailing were conducted on 6 ng of CUT&RUN eluted DNA for 30 min at 20°C followed by 1 hour at 50°C. After adaptor ligation for 30 min at 20°C, the DNA fragments were purified by 1.75× volume of AMPure XP beads (Beckman Coulter) followed by 10 to 12 cycles of PCR amplification with Next Ultra II Q5 master mix. The PCR products were purified with 1× volume of AMPure XP beads. After quantitative and qualitative analysis, libraries with different indexes were pooled and sequenced on Illumina NovaSeq platform with paired-end 150-bp reads.

CUT&RUN data processing
CUT&RUN sequencing data were analyzed as described previously (74), following the standard pipeline (https://yezhengstat.github.io/CUTTag_tutorial/index.html). Briefly, paired-end 150-bp reads were aligned to GRCh38 human genome using Bowtie2 version 2.2.5 (75) with the following options: --local --very-sensitive --no-mixed --no-discordant --phred33 -I 10 -X 700. Technical replicates ($n = 4$ per condition) were merged before read alignment to increase the power of peak calling. macs2 (76) was used to call peaks from bam files. For SOX9 CUT&RUN peak calling, parameters —t input_file −p 1e-5 −f BAM −keep-dup all −n out_name was used to call narrow peaks. To check the SOX9 binding profile and enhancer activity of specific gene sets, proximal peaks (−2 kb to 2 kb relative to TSS) called by MACS2 were linked/annotated to genes by ChIP-seeker version 1.34.1 (77). Then, computeMatrix and plotHeatmap functions from deepTools (78) were used to visualize peaks.

Intestinal organoid culture
Colonic glands were isolated, treated with EDTA, and then resuspended in 30 to 50 µl of Matrigel (BD Bioscience) and plated in 24-well plates. WRN containing DMEM/F12 with Hepes (Sigma-Aldrich) containing 20% FBS, 1% penicillin-streptomycin, and recombinant mouse epidermal growth factor (50 ng/ml; Life Technologies) was used for culturing Apc^{KO} colon organoids. For the first 2 to 3 days after seeding, the medium was also supplemented with 10 mM ROCK inhibitor Y-27632 (Sigma-Aldrich) and 10 mM SB431542 (Sigma-Aldrich), an inhibitor for the transforming growth factor−β (TGF-β) type I receptor to avoid anoikis. For passage, colon organoids were dispersed by trypsin-EDTA and transferred to fresh Matrigel. Passage was performed every 3 to 4 days with a 1:3 to 1:5 split ratio. For human colon organoid culture, the previous medium was supplemented with antibiotics Primocin (100 µg/ml; InvivoGen) and Normocin (100 µg/ml; InvivoGen), serum-free supplements 1× B27 [Thermo Fisher Scientific (Gibco)] and 1× N2 [Thermo Fisher Scientific (Gibco)], chemical supplements 10 mM nicotinamide (Sigma-Aldrich) and 500 mM *N*-acetyl cysteine (Sigma-Aldrich), hormone 50 mM [Leu15]-Gastrin (Sigma-Aldrich), growth factor FGF10 (100 µg/ml; recombinant human; Thermo Fisher Scientific), and 500 nM A-83-01 (Sigma-Aldrich), which is an inhibitor of the TGF-β receptors ALK4, ALK5, and ALK7.

Organoid fixation for FFPE
Confluent organoids in six-well plate were fixed in 10% formalin at 4°C on rocker overnight. The fixed organoids were washed with PBS, collected by centrifugation at 2000 rpm for 3 min. The supernatant was carefully aspirated; cell pellets were resuspended in 50 to 80 µl of 2% agar and then immediately kept on ice. The solidified agar with organoids was kept in a cassette and processed to make formalin fixed paraffin embedded (FFPE) blocks.

Cell proliferation assays
Cell viability was quantified by measuring cellular adenosine triphosphate content using the CTG Cell Viability assay (Promega) according to the manufacturer's instructions. All experiments were performed in triplicate in 96-well plates.

SOX9 recombination PCR
Mouse tails were incubated at 95°C in 75 µl of the cell lysis buffer [5 ml of sterile ddH$_2$O, 7 µl of 50% NaOH, and 7 µl of 0.5 M EDTA (pH 8.0)], followed by 15 min at 4°C, and neutralized with 75 µl of neutralization buffer [40 mM tris-HCl (pH ~5)]. Supernatant (2 µl) was used for PCR amplification using primers designed for WT SOX9 and unfloxed SOX9 and floxed SOX9 (table S4) using Phire Tissue

Direct PCR master mix (Thermo Fisher Scientific, #F170S). PCR cycling conditions were initial denaturation [94°C, 120 s; 10× touchdown cycles with the following three steps: 94°C, 10 s; 65°C (0.5°C increment each cycle), 10 s; and 72°C, 90 s; 25× cycles with the following three steps: 94°C, 10 s; 60°C, 10 s; and 72°C, 90 s; the last annealing: 72°C, 180 s]. The PCR products were analyzed on 1% agarose gel.

Organoid adenoviral transduction
To transduce colonic organoids, 0.5 M organoids were suspended in 500 μl of WRN medium with 10 μM Y27632 ROCK inhibitor in a 24-well ultralow attachment plate. Adenovirus (University of Iowa, Gene Transfer Vector Core, stock: Ad3786; high viral titer equal to 1010 plaque-forming units/ml) carrying GFP or GFP-Cre (1 μl) was added to the organoids, and the sealed plate is centrifuged at 600g for 1 hour at 32°C, followed by incubation at 37°C for 5 to 6 hours. After incubation, the transduced organoids were washed with complete medium and resuspended in about 200 μl of Matrigel and plated in Nunclon delta plates with WRN conditioned media with 10 μM ROCK inhibitor.

Generation of stable colon organoids
All genetically manipulated colon organoid lines were generated using the protocol described here (79). shRNAs against SOX9 were cloned into PLKO.1, TET-PLKO, and TET-Cellecta vectors. To generate lentiviruses, expression vectors were cotransfected into HEK293T cells with the lentiviral packaging constructs psPAX2 and pMD2.G (vesicular stomatitis virus glycoprotein) in a 1:1:1 ratio using X-tremeGENE 9 DNA Transfection Reagent (Roche) according to the manufacturer's instructions. Cell culture medium was changed the following day, and lentiviral supernatant was harvested 48 and 72 hours later and filtered through a 0.45-μm filter (Millipore). Lentiviruses were aliquoted and stored at −80°C until use.

To transduce colonic organoids, spheroids in one well (24-well plate) were trypsinized, and a one-fourth to one-eighth volume of cell suspension was used for each infection. Cells were resuspended in 500 μl of lentiviral supernatant with polybrene (8 μg/ml) and 10 mM Y-27632, centrifuged at 600g at 32°C for 1 hour, and incubated for 6 hours in a cell culture incubator. The infected cells were suspended in 30 to 50 μl of Matrigel and cultured with Wnt/R-spondin−deprived medium containing 10 mM Y-27632 and 10 mM SB431542. Colon organoids were selected with puromycin (3 μg/ml) at 24 hours after infection.

RNA isolation and qPCR
Total RNA was isolated using the RNeasy Mini Kit (QIAGEN, Germantown, MD, USA), and cDNA was synthesized using the iScript Reverse Transcription Supermix for RT-qPCR (Bio-Rad) according to the manufacturer's instructions. Gene-specific primers for SYBR Green real-time PCR were either obtained from previously published sequences or designed by Primer-BLAST (www.ncbi.nlm.nih.gov/tools/primer-blast/) and synthesized by Integrated DNA Technologies or ETON Bioscience. Real-time PCR was performed and analyzed using CFX96 Real-Time PCR Detection System (Bio-Rad Laboratories Inc., Hercules, CA) and using Power SYBR Green PCR Master Mix (Thermo Fisher Scientific) according to the manufacturer's instructions. Relative mRNA expression was determined by normalizing to *GAPDH* expression, which served as an internal control. See table S4 for primers used for qPCR.

Immunoblot, antibodies, and inhibitors
Immunoblot analysis was performed as previously described (80). Briefly, cells were lysed in radioimmunoprecipitation assay buffer supplemented with a protease inhibitor cocktail (Roche). Whole-cell extracts were resolved by SDS–polyacrylamide gel electrophoresis, transferred to polyvinylidene difluoride membranes, and probed with indicated primary antibodies. Bound antibodies were detected with horseradish peroxidase (HRP)−conjugated secondary antibodies and chemiluminescent HRP substrate. The following primary antibodies were used for Western blotting (all from CST, Beverly, MA, USA, unless otherwise indicated): anti-SOX9 (#82630; 1:1000), anti-vinculin (#13901; 1:1000), and anti-RFP (Rockland, 600-401-379; 1:500).

Statistical analysis and reproducibility
Experiments were performed in triplicate. Data are represented as means ± SD unless indicated otherwise. For each experiment, either independent biological or technical replicates are as noted in the figure legends and were repeated with similar results. Statistical analysis was performed using Microsoft Office, Prism 7.0 (Graph-Pad), or RStudio statistical tools. Pairwise comparisons between groups (that is, experimental versus control) were performed using an unpaired two-tailed Student's t test or Kruskal-Wallis test as appropriate unless otherwise indicated. For all experiments, the variance between comparison groups was found to be equivalent. Animals were excluded from analysis if they were euthanized because of health reasons unrelated to tumor volume end point.

REFERENCES AND NOTES
1. K. K. Banerjee, M. Saxena, N. Kumar, L. Chen, A. Cavazza, N. H. Toke, N. K. O'Neill, S. Madha, U. Jadhav, M. P. Verzi, R. A. Shivdasani, Enhancer, transcriptional, and cell fate plasticity precedes intestinal determination during endoderm development. *Genes Dev.* **32**, 1430–1442 (2018).
2. F. de Sousa E Melo, F. J. de Sauvage, Cellular plasticity in intestinal homeostasis and disease. *Cell Stem Cell* **24**, 54–64 (2019).
3. D. Shlyueva, G. Stampfel, A. Stark, Transcriptional enhancers: From properties to genome-wide predictions. *Nat. Rev. Genet.* **15**, 272–286 (2014).
4. I. Arozarena, C. Wellbrock, Phenotype plasticity as enabler of melanoma progression and therapy resistance. *Nat. Rev. Cancer* **19**, 377–391 (2019).
5. P. B. Gupta, I. Pastushenko, A. Skibinski, C. Blanpain, C. Kuperwasser, Phenotypic plasticity: driver of cancer initiation, progression, and therapy resistance. *Cell Stem Cell* **24**, 65–78 (2019).
6. D. Hanahan, Hallmarks of cancer: New dimensions. *Cancer Discov.* **12**, 31–46 (2022).
7. W. A. Flavahan, E. Gaskell, B. E. Bernstein, Epigenetic plasticity and the hallmarks of cancer. *Science* **357**, (2017).
8. K. Ganesh, H. Basnet, Y. Kaygusuz, A. M. Laughney, L. He, R. Sharma, K. P. O'Rourke, V. P. Reuter, Y. H. Huang, M. Turkekul, E. E. Er, I. Masilionis, K. Manova-Todorova, M. R. Weiser, L. B. Saltz, J. Garcia-Aguilar, R. Koche, S. W. Lowe, D. Pe'er, J. Shia, J. Massagué, L1CAM

defines the regenerative origin of metastasis-initiating cells in colorectal cancer. *Nat. Cancer* **1**, 28–45 (2020).

9. X. Liang, G. N. Duronio, Y. Yang, P. Bala, P. Hebbar, S. Spisak, P. Sahgal, H. Singh, Y. Zhang, Y. Xie, P. Cejas, H. W. Long, A. J. Bass, N. S. Sethi, An enhancer-driven stem cell-like program mediated by SOX9 blocks intestinal differentiation in colorectal cancer. *Gastroenterology* **162**, 209–222 (2022).

10. T. Sato, R. G. Vries, H. J. Snippert, M. van de Wetering, N. Barker, D. E. Stange, J. H. van Es, A. Abo, P. Kujala, P. J. Peters, H. Clevers, Single Lgr5 stem cells build crypt-villus structures in vitro without a mesenchymal niche. *Nature* **459**, 262–265 (2009).

11. L. Chen, N. H. Toke, S. Luo, R. P. Vasoya, R. L. Fullem, A. Parthasarathy, A. O. Perekatt, M. P. Verzi, A reinforcing HNF4-SMAD4 feed-forward module stabilizes enterocyte identity. *Nat. Genet.* **51**, 777–785 (2019).

12. Z. Qi, Y. Li, B. Zhao, C. Xu, Y. Liu, H. Li, B. Zhang, X. Wang, X. Yang, W. Xie, B. Li, J. D. J. Han, Y. G. Chen, BMP restricts stemness of intestinal Lgr5+ stem cells by directly suppressing their signature genes. *Nat. Commun.* **8**, 13824 (2017).

13. J. Kazakevych, S. Sayols, B. Messner, C. Krienke, N. Soshnikova, Dynamic changes in chromatin states during specification and differentiation of adult intestinal stem cells. *Nucleic Acids Res.* **45**, 5770–5784 (2017).

14. T. H. Kim, F. Li, I. Ferreiro-Neira, L. L. Ho, A. Luyten, K. Nalapareddy, H. Long, M. Verzi, R. A. Shivdasani, Broadly permissive intestinal chromatin underlies lateral inhibition and cell plasticity. *Nature* **506**, 511–515 (2014).

15. R. L. Siegel, K. D. Miller, A. Jemal, Cancer statistics, 2018. *CA Cancer J. Clin.* **68**, 7–30 (2018).

16. A. K. Rustgi, Molecular genetics and colorectal cancer. *Gastroenterology* **104**, 1223–1225 (1993).

17. W. R. Becker, S. A. Nevins, D. C. Chen, R. Chiu, A. M. Horning, T. K. Guha, R. Laquindanum, M. Mills, H. Chaib, U. Ladabaum, T. Longacre, J. Shen, E. D. Esplin, A. Kundaje, J. M. Ford, C. Curtis, M. P. Snyder, W. J. Greenleaf, Single-cell analyses define a continuum of cell state and composition changes in the malignant transformation of polyps to colorectal cancer. *Nat. Genet.* **54**, 985–995 (2022).

18. E. R. Fearon, B. Vogelstein, A genetic model for colorectal tumorigenesis. *Cell* **61**, 759–767 (1990).

19. K. W. Kinzler, M. C. Nilbert, L. K. Su, B. Vogelstein, T. M. Bryan, D. B. Levy, K. J. Smith, A. C. Preisinger, P. Hedge, D. McKechnie, R. Finniear, A. Markham, J. Groffen, M. S. Boguski, S. F. Altschul, A. Horii, Y. Ando, Y. Miyoshi, Y. Miki, I. Nishisho, Y. Nakamura, Identification of FAP locus genes from chromosome 5q21. *Science* **253**, 661–665 (1991).

20. Y. Xing, W. K. Clements, D. Kimelman, W. Xu, Crystal structure of a β-catenin/axin complex suggests a mechanism for the β-catenin destruction complex. *Genes Dev.* **17**, 2753–2764 (2003).

21. N. C. Ha, T. Tonozuka, J. L. Stamos, H. J. Choi, W. I. Weis, Mechanism of phosphorylation-dependent binding of APC to β-catenin and its role in β-catenin degradation. *Mol. Cell* **15**, 511–521 (2004).

22. S. Munemitsu, I. Albert, B. Souza, B. Rubinfeld, P. Polakis, Regulation of intracellular beta-catenin levels by the adenomatous polyposis coli (APC) tumor-suppressor protein. *Proc. Natl. Acad. Sci. U.S.A.* **92**, 3046–3050 (1995).

23. H. C. Korswagen, D. Y. M. Coudreuse, M. C. Betist, S. van de Water, D. Zivkovic, H. C. Clevers, The Axin-like protein PRY-1 is a negative regulator of a canonical Wnt pathway in *C. elegans*. *Genes Dev.* **16**, 1291–1302 (2002).

24. M. van Noort, J. Meeldijk, R. van der Zee, O. Destree, H. Clevers, Wnt signaling controls the phosphorylation status of β-catenin. *J. Biol. Chem.* **277**, 17901–17905 (2002).

25. V. Korinek, N. Barker, P. J. Morin, D. van Wichen, R. de Weger, K. W. Kinzler, B. Vogelstein, H. Clevers, Constitutive transcriptional activation by a β-catenin-Tcf complex in APC−/− colon carcinoma. *Science* **275**, 1784–1787 (1997).

26. P. J. Morin, A. B. Sparks, V. Korinek, N. Barker, H. Clevers, B. Vogelstein, K. W. Kinzler, Activation of β-catenin-Tcf signaling in colon cancer by mutations in β-catenin or APC. *Science* **275**, 1787–1790 (1997).

27. L. E. Dow, K. P. O'Rourke, J. Simon, D. F. Tschaharganeh, J. H. van Es, H. Clevers, S. W. Lowe, Apc restoration promotes cellular differentiation and reestablishes crypt homeostasis in colorectal cancer. *Cell* **161**, 1539–1552 (2015).

28. M. C. Faux, J. L. Ross, C. Meeker, T. Johns, H. Ji, R. J. Simpson, M. J. Layton, A. W. Burgess, Restoration of full-length adenomatous polyposis coli (APC) protein in a colon cancer cell line enhances cell adhesion. *J. Cell Sci.* **117**, 427–439 (2004).

29. J. Groden, G. Joslyn, W. Samowitz, D. Jones, N. Bhattacharyya, L. Spirio, A. Thliveris, M. Robertson, S. Egan, M. Meuth, Response of colon cancer cell lines to the introduction of APC, a colon-specific tumor suppressor gene. *Cancer Res.* **55**, 1531–1539 (1995).

30. F. de Sousa e Melo, A. V. Kurtova, J. M. Harnoss, N. Kljavin, J. D. Hoeck, J. Hung, J. E. Anderson, E. E. Storm, Z. Modrusan, H. Koeppen, G. J. P. Dijkgraaf, R. Piskol, F. J. de Sauvage, A distinct role for Lgr5+ stem cells in primary and metastatic colon cancer. *Nature* **543**, 676–680 (2017).

31. M. Shimokawa, Y. Ohta, S. Nishikori, M. Matano, A. Takano, M. Fujii, S. Date, S. Sugimoto, T. Kanai, T. Sato, Visualization and targeting of LGR5+ human colon cancer stem cells. *Nature* **545**, 187–192 (2017).

32. N. Barker, H. Clevers, Mining the Wnt pathway for cancer therapeutics. *Nat. Rev. Drug Discov.* **5**, 997–1014 (2006).

33. S. Colnot, T. Decaens, M. Niwa-Kawakita, C. Godard, G. Hamard, A. Kahn, M. Giovannini, C. Perret, Liver-targeted disruption of Apc in mice activates β-catenin signaling and leads to hepatocellular carcinomas. *Proc. Natl. Acad. Sci. U.S.A.* **101**, 17216–17221 (2004).

34. A. G. Schepers, H. J. Snippert, D. E. Stange, M. van den Born, J. H. van Es, M. van de Wetering, H. Clevers, Lineage tracing reveals Lgr5+ stem cell activity in mouse intestinal adenomas. *Science* **337**, 730–735 (2012).

35. O. J. Sansom, K. R. Reed, A. J. Hayes, H. Ireland, H. Brinkmann, I. P. Newton, E. Batlle, P. Simon-Assmann, H. Clevers, I. S. Nathke, A. R. Clarke, D. J. Winton, Loss of Apc in vivo immediately perturbs Wnt signaling, differentiation, and migration. *Genes Dev.* **18**, 1385–1390 (2004).

36. A. E. Powell, Y. Wang, Y. Li, E. J. Poulin, A. L. Means, M. K. Washington, J. N. Higginbotham, A. Juchheim, N. Prasad, S. E. Levy, Y. Guo, Y. Shyr, B. J. Aronow, K. M. Haigis, J. L. Franklin, R. J. Coffey, The pan-ErbB negative regulator Lrig1 is an intestinal stem cell marker that functions as a tumor suppressor. *Cell* **149**, 146–158 (2012).

37. J. H. van Es, M. E. van Gijn, O. Riccio, M. van den Born, M. Vooijs, H. Begthel, M. Cozijnsen, S. Robine, D. J. Winton, F. Radtke, H. Clevers, Notch/gamma-secretase inhibition turns proliferative cells in intestinal crypts and adenomas into goblet cells. *Nature* **435**, 959–963 (2005).

38. A. L. Haber, M. Biton, N. Rogel, R. H. Herbst, K. Shekhar, C. Smillie, G. Burgin, T. M. Delorey, M. R. Howitt, Y. Katz, I. Tirosh, S. Beyaz, D. Dionne, M. Zhang, R. Raychowdhury, W. S. Garrett, O. Rozenblatt-Rosen, H. N. Shi, O. Yilmaz, R. J. Xavier, A. Regev, A single-cell survey of the small intestinal epithelium. *Nature* **551**, 333–339 (2017).

39. Y. Feng, K. Sentani, A. Wiese, E. Sands, M. Green, G. T. Bommer, K. R. Cho, E. R. Fearon, Sox9 induction, ectopic Paneth cells, and mitotic spindle axis defects in mouse colon adenomatous epithelium arising from conditional biallelic Apc inactivation. *Am. J. Pathol.* **183**, 493–503 (2013).

40. E. Sancho, E. Batlle, H. Clevers, Signaling pathways in intestinal development and cancer. *Annu. Rev. Cell Dev. Biol.* **20**, 695–723 (2004).

41. J. Munoz, D. E. Stange, A. G. Schepers, M. van de Wetering, B.-K. Koo, S. Itzkovitz, R. Volckmann, K. S. Kung, J. Koster, S. Radulescu, K. Myant, R. Versteeg, O. J. Sansom, J. H. van Es, N. Barker, A. van Oudenaarden, S. Mohammed, A. J. R. Heck, H. Clevers, The Lgr5 intestinal stem cell signature: robust expression of proposed quiescent '+4' cell markers. *EMBO J.* **31**, 3079–3091 (2012).

42. Y. M. Nusse, A. K. Savage, P. Marangoni, A. K. M. Rosendahl-Huber, T. A. Landman, F. J. de Sauvage, R. M. Locksley, O. D. Klein, Parasitic helminths induce fetal-like reversion in the intestinal stem cell niche. *Nature* **559**, 109–113 (2018).

43. J. D. Buenrostro, P. G. Giresi, L. C. Zaba, H. Y. Chang, W. J. Greenleaf, Transposition of native chromatin for fast and sensitive epigenomic profiling of open chromatin, DNA-binding proteins and nucleosome position. *Nat. Methods* **10**, 1213–1218 (2013).

44. W. J. McKinstry, C. L. Li, E. J. J. Rasko, N. A. Nicola, G. R. Johnson, D. Metcalf, Cytokine receptor expression on hematopoietic stem and progenitor cells. *Blood* **89**, 65–71 (1997).

45. M. Joosten, P. J. M. Valk, M. A. Jordà, Y. Vankan-Berkhoudt, S. Verbakel, M. van den Broek, A. Beijen, B. Löwenberg, R. Delwel, Leukemic predisposition of pSca-1/Cb2 transgenic mice. *Exp. Hematol.* **30**, 142–149 (2002).

46. T. S. Fenske, C. Pengue, V. Mathews, P. T. Hanson, S. E. Hamm, N. Riaz, T. A. Graubert, Stem cell expression of the AML1/ETO fusion protein induces a myeloproliferative disorder in mice. *Proc. Natl. Acad. Sci. U.S.A.* **101**, 15184–15189 (2004).

47. V. Fernandez Vallone, M. Leprovots, S. Strollo, G. Vasile, A. Lefort, F. Libert, G. Vassart, M. I. Garcia, Trop2 marks transient gastric fetal epithelium and adult regenerating cells after epithelial damage. *Development* **143**, 1452–1463 (2016).

48. R. C. Mustata, G. Vasile, V. Fernandez-Vallone, S. Strollo, A. Lefort, F. Libert, D. Monteyne, D. Pérez-Morga, G. Vassart, M. I. Garcia, Identification of Lgr5-independent spheroid-generating progenitors of the mouse fetal intestinal epithelium. *Cell Rep.* **5**, 421–432 (2013).

49. L. Chen, Z. Luo, C. Zhao, Q. Li, Y. Geng, Y. Xiao, M.-K. Chen, L. Li, Z.-X. Chen, M. Wu, Dynamic chromatin states coupling with key transcription factors in colitis-associated colorectal cancer. *Adv. Sci.* **9**, 2200536 (2022).

50. H. F. Vasen, G. Möslein, A. Alonso, I. Aretz, I. Bernstein, L. Bertario, I. Blanco, S. Bülow, J. Burn, G. Capella, C. Colas, C. Engel, I. Frayling, W. Friedl, F. J. Hes, S. Hodgson, H. Järvinen, J.-P. Mecklin, P. Møller, T. Myrhøi, F. M. Nagengast, Y. Parc, R. Phillips, S. K. Clark, M. Ponz de Leon, L. Renkonen-Sinisalo, J. R. Sampson, A. Stormorken, S. Tejpar, H. J. W. Thomas, J. Wijnen, Guidelines for the clinical management of familial adenomatous polyposis (FAP). *Gut* **57**, 704–713 (2008).

51. M. Ranes, M. Zaleska, S. Sakalas, R. Knight, S. Guettler, Reconstitution of the destruction complex defines roles of AXIN polymers and APC in β-catenin capture, phosphorylation, and ubiquitylation. *Mol. Cell* **81**, 3246–3261.e11 (2021).

52. I. Lukonin, D. Serra, L. Challet Meylan, K. Volkmann, J. Baaten, R. Zhao, S. Meeusen, K. Colman, F. Maurer, M. B. Stadler, J. Jenkins, P. Liberali, Phenotypic landscape of intestinal organoid regeneration. *Nature* **586**, 275–280 (2020).

53. H. Akiyama, M. C. Chaboissier, J. F. Martin, A. Schedl, B. de Crombrugghe, The transcription factor Sox9 has essential roles in successive steps of the chondrocyte differentiation pathway and is required for expression of Sox5 and Sox6. *Genes Dev.* **16**, 2813–2828 (2002).

54. K. Flanagan, Z. Modrusan, J. Cornelius, A. Chavali, I. Kasman, L. Komuves, L. Mo, L. Diehl, Intestinal epithelial cell up-regulation of LY6 molecules during colitis results in enhanced chemokine secretion. *J. Immunol.* **180**, 3874–3881 (2008).

55. S. Yui, L. Azzolin, M. Maimets, M. T. Pedersen, R. P. Fordham, S. L. Hansen, H. L. Larsen, J. Guiu, M. R. P. Alves, C. F. Rundsten, J. V. Johansen, Y. Li, C. D. Madsen, T. Nakamura, M. Watanabe, O. H. Nielsen, P. J. Schweiger, S. Piccolo, K. B. Jensen, yap/taz-dependent reprogramming of colonic epithelium links ECM remodeling to tissue regeneration. *Cell Stem Cell* **22**, 35–49.e7 (2018).

56. K. Murata, U. Jadhav, S. Madha, J. van Es, J. Dean, A. Cavazza, K. Wucherpfennig, F. Michor, H. Clevers, R. A. Shivdasani, Ascl2-dependent cell dedifferentiation drives regeneration of ablated intestinal stem cells. *Cell Stem Cell* **26**, 377–390.e6 (2020).

57. M. Hu, R. A. Shivdasani, Overlapping gene expression in fetal mouse intestine development and human colorectal cancer. *Cancer Res.* **65**, 8715–8722 (2005).

58. M. M. Pomerantz, X. Qiu, Y. Zhu, D. Y. Takeda, W. Pan, S. C. Baca, A. Gusev, K. D. Korthauer, T. M. Severson, G. Ha, S. R. Viswanathan, J. H. Seo, H. M. Nguyen, B. Zhang, B. Pasaniuc, C. Giambartolomei, S. A. Alaiwi, C. A. Bell, E. P. O'Connor, M. S. Chabot, D. R. Stillman, R. Lis, A. Font-Tello, L. Li, P. Cejas, A. M. Bergman, J. Sanders, H. G. van der Poel, S. A. Gayther, K. Lawrenson, M. A. S. Fonseca, J. Reddy, R. I. Corona, G. Martovetsky, B. Egan, T. Choueiri, L. Ellis, I. P. Garraway, G. S. M. Lee, E. Corey, H. W. Long, W. Zwart, M. L. Freedman, Prostate cancer reactivates developmental epigenomic programs during metastatic progression. *Nat. Genet.* **52**, 790–799 (2020).

59. Q. Weng, J. Wang, J. Wang, D. He, Z. Cheng, F. Zhang, R. Verma, L. Xu, X. Dong, Y. Liao, X. He, A. Potter, L. Zhang, C. Zhao, M. Xin, Q. Zhou, B. J. Aronow, P. J. Blackshear, J. N. Rich, Q. He, W. Zhou, M. L. Suvà, R. R. Waclaw, S. S. Potter, G. Yu, Q. R. Lu, Single-cell transcriptomics uncovers glial progenitor diversity and cell fate determinants during development and gliomagenesis. *Cell Stem Cell* **24**, 707–723.e8 (2019).

60. H. Graffner, B. Hultberg, B. Johansson, T. Moller, B. G. Petersson, Detection of recurrent cancer of the colon and rectum. *J. Surg. Oncol.* **28**, 156–159 (1985).

61. J. J. Szymendera, M. P. Nowacki, A. W. Szawlowski, J. A. Kaminska, Predictive value of plasma CEA levels. *Dis. Colon Rectum* **25**, 46–52 (1982).

62. M. van der Heijden, L. Vermeulen, Stem cells in homeostasis and cancer of the gut. *Mol. Cancer* **18**, 66 (2019).

63. A. Fumagalli, K. C. Oost, L. Kester, J. Morgner, L. Bornes, L. Bruens, L. Spaargaren, M. Azkanaz, T. Schelfhorst, E. Beerling, M. C. Heinz, D. Postrach, D. Seinstra, A. M. Sieuwerts, J. W. M. Martens, S. van der Elst, M. van Baalen, D. Bhowmick, N. Vrisekoop, S. I. J. Ellenbroek, S. J. E. Suijkerbuijk, H. J. Snippert, J. van Rheenen, Plasticity of Lgr5-negative cancer cells drives metastasis in colorectal cancer. *Cell Stem Cell*, **26**, 569–578.e7 (2020).

64. C. Albuquerque, C. Breukel, R. van der Luijt, P. Fidalgo, P. Lage, F. J. Slors, C. N. Leitão, R. Fodde, R. Smits, The 'just-right' signaling model: APC somatic mutations are selected based on a specific level of activation of the β-catenin signaling cascade. *Hum. Mol. Genet.* **11**, 1549–1560 (2002).

65. H. de The, Differentiation therapy revisited. *Nat. Rev. Cancer* **18**, 117–127 (2018).

66. P. Ordonez-Moran, C. Dafflon, M. Imajo, E. Nishida, J. Huelsken, HOXA5 counteracts stem cell traits by inhibiting Wnt signaling in colorectal cancer. *Cancer Cell* **28**, 815–829 (2015).

67. K. C. Roche, A. D. Gracz, X. F. Liu, V. Newton, H. Akiyama, S. T. Magness, SOX9 maintains reserve stem cells and preserves radioresistance in mouse small intestine. *Gastroenterology* **149**, 1553–1563.e10 (2015).

68. L. Hou, Y. Srivastava, R. Jauch, Molecular basis for the genome engagement by Sox proteins. *Semin. Cell Dev. Biol.* **63**, 2–12 (2017).

69. N. Barker, J. H. van Es, J. Kuipers, P. Kujala, M. van den Born, M. Cozijnsen, A. Haegebarth, J. Korving, H. Begthel, P. J. Peters, H. Clevers, Identification of stem cells in small intestine and colon by marker gene Lgr5. *Nature* **449**, 1003–1007 (2007).

70. L. Madisen, T. A. Zwingman, S. M. Sunkin, S. W. Oh, H. A. Zariwala, H. Gu, L. L. Ng, R. D. Palmiter, M. J. Hawrylycz, A. R. Jones, E. S. Lein, H. Zeng, A robust and high-throughput Cre reporting and characterization system for the whole mouse brain. *Nat. Neurosci.* **13**, 133–140 (2010).

71. C. Neufert, C. Becker, M. F. Neurath, An inducible mouse model of colon carcinogenesis for the analysis of sporadic and inflammation-driven tumor progression. *Nat. Protoc.* **2**, 1998–2004 (2007).

72. M. R. Corces, A. E. Trevino, E. G. Hamilton, P. G. Greenside, N. A. Sinnott-Armstrong, S. Vesuna, A. T. Satpathy, A. J. Rubin, K. S. Montine, B. Wu, A. Kathiria, S. W. Cho, M. R. Mumbach, A. C. Carter, M. Kasowski, L. A. Orloff, V. I. Risca, A. Kundaje, P. A. Khavari, T. J. Montine, W. J. Greenleaf, H. Y. Chang, An improved ATAC-seq protocol reduces background and enables interrogation of frozen tissues. *Nat. Methods* **14**, 959–962 (2017).

73. P. J. Skene, S. Henikoff, An efficient targeted nuclease strategy for high-resolution mapping of DNA binding sites. *eLife* **6**, (2017).

74. P. J. Skene, J. G. Henikoff, S. Henikoff, Targeted in situ genome-wide profiling with high efficiency for low cell numbers. *Nat. Protoc.* **13**, 1006–1019 (2018).

75. B. Langmead, S. L. Salzberg, Fast gapped-read alignment with Bowtie 2. *Nat. Methods* **9**, 357–359 (2012).

76. Y. Zhang, T. Liu, C. A. Meyer, J. Eeckhoute, D. S. Johnson, B. E. Bernstein, C. Nusbaum, R. M. Myers, M. Brown, W. Li, X. S. Liu, Model-based analysis of ChIP-Seq (MACS). *Genome Biol.* **9**, R137 (2008).

77. Q. Wang, M. Li, T. Wu, L. Zhan, L. Li, M. Chen, W. Xie, Z. Xie, E. Hu, S. Xu, G. Yu, Exploring epigenomic datasets by ChIPseeker. *Curr. Protoc.* **2**, e585 (2022).

78. F. Ramírez, D. P. Ryan, B. Grüning, V. Bhardwaj, F. Kilpert, A. S. Richter, S. Heyne, F. Dündar, T. Manke, deepTools2: A next generation web server for deep-sequencing data analysis. *Nucleic Acids Res.* **44**, W160–W165 (2016).

79. O. Shalem, N. E. Sanjana, E. Hartenian, X. Shi, D. A. Scott, T. S. Mikkelsen, D. Heckl, B. L. Ebert, D. E. Root, J. G. Doench, F. Zhang, Genome-scale CRISPR-Cas9 knockout screening in human cells. *Science* **343**, 84–87 (2014).

80. G. S. Wong, J. Zhou, J. B. Liu, Z. Wu, X. Xu, T. Li, D. Xu, S. E. Schumacher, J. Puschhof, J. McFarland, C. Zou, A. Dulak, L. Henderson, P. Xu, E. O'Day, R. Rendak, W. L. Liao, F. Cecchi, T. Hembrough, S. Schwartz, C. Szeto, A. K. Rustgi, K. K. Wong, J. A. Diehl, K. Jensen, F. Graziano, A. Ruzzo, S. Fereshetian, P. Mertins, S. A. Carr, R. Beroukhim, K. Nakamura, E. Oki, M. Watanabe, H. Baba, Y. Imamura, D. Catenacci, A. J. Bass, Targeting wild-type KRAS-amplified gastroesophageal cancer through combined MEK and SHP2 inhibition. *Nat. Med.* **24**, 968–977 (2018).